

Tensor Recovery Based on A Novel Non-convex Function Minimax Logarithmic Concave Penalty Function

Hongbing Zhang, Xinyi Liu, Chang Liu, Hongtao Fan, Yajing Li, Xinyun Zhu

Abstract—Non-convex relaxation methods have been widely used in tensor recovery problems, and compared with convex relaxation methods, can achieve better recovery results. In this paper, a new non-convex function, Minimax Logarithmic Concave Penalty (MLCP) function, is proposed, and some of its intrinsic properties are analyzed, among which it is interesting to find that the Logarithmic function is an upper bound of the MLCP function. The proposed function is generalized to tensor cases, yielding tensor MLCP and weighted tensor L_γ -norm. Consider that its explicit solution cannot be obtained when applying it directly to the tensor recovery problem. Therefore, the corresponding equivalence theorems to solve such problem are given, namely, tensor equivalent MLCP theorem and equivalent weighted tensor L_γ -norm theorem. In addition, we propose two EMLCP-based models for classic tensor recovery problems, namely low-rank tensor completion (LRTC) and tensor robust principal component analysis (TRPCA), and design proximal alternate linearization minimization (PALM) algorithms to solve them individually. Furthermore, based on the Kurdyka-Lojasiewicz property, it is proved that the solution sequence of the proposed algorithm has finite length and converges to the critical point globally. Finally, Extensive experiments show that proposed algorithm achieve good results, and it is confirmed that the MLCP function is indeed better than the Logarithmic function in the minimization problem, which is consistent with the analysis of theoretical properties.

Index Terms—Minimax logarithmic concave penalty (MLCP), equivalent weighted Tensor L_γ -norm, low-rank tensor completion (LRTC), tensor robust principal component analysis (TRPCA).

I. INTRODUCTION

DATA structures become more complex, and the processing required by many applications becomes more difficult as the dimensionality of the data increases. As a representation of multi-dimensional data, tensors have played an important role in many high-dimensional data applications in recent years, such as color image/video (CI/CV) processing [1], [2], [3], [4], hyperspectral/multispectral image (HSI/MSI)

This work was supported by the National Natural Science Foundation of China (Nos. 11701456, 11801452, 11571004), Fundamental Research Project of Natural Science in Shaanxi Province General Project (Youth) (Nos. 2019JQ-415, 2019JQ-196), the Initial Foundation for Scientific Research of Northwest A&F University (Nos.2452017219, 2452018017), and Innovation and Entrepreneurship Training Program for College Students of Shaanxi Province (S201910712132).

H. Zhang, X. Liu, C. Liu, H. Fan and Y. Li are with Department of information and Computing Science, College of Science, Northwest A&F University, Yangling, Shaanxi 712100, China(e-mail: zhanghb@nwfau.edu.cn; Lxy6x1@163.com; chang_10923@163.com ; fanht17@nwfau.edu.cn; hliyajing@163.com).

X. Zhu is with the Department of Mathematics, University of Texas of the Permian Basin, Odessa, TX 79762, USA(e-mail: zhu_x@utpb.edu).

processing [5], [6], [7], [8], magnetic resonance imaging (MRI) data recovery [9], [10], [11], [12], video foreground and background subtraction[13], [14], [15], [16], video rain stripe removal [17], [18], and signal reconstruction [19], [20].

These practical application problems above can be transformed into tensor recovery problems. For different observation data, the tensor recovery problem can usually be modeled as a low-rank tensor completion (LRTC) problem and a tensor robust principal component analysis (TRPCA) problem. Their corresponding models are as follows:

$$\min_{\mathcal{Z}} \text{rank}(\mathcal{Z}) \quad \text{s.t. } P_{\Omega}(\mathcal{T}) = P_{\Omega}(\mathcal{Z}) \quad (1)$$

$$\min_{\mathcal{Z}, \mathcal{E}} \text{rank}(\mathcal{Z}) + \tau_1 \|\mathcal{E}\|_1 \quad \text{s.t. } \mathcal{T} = \mathcal{Z} + \mathcal{E}, \quad (2)$$

where $\mathcal{T} \in \mathbb{R}^{I_1 \times I_2 \times I_3}$ is the observation; \mathcal{Z} is initial tensor; \mathcal{E} is sparsity tensor; $P_{\Omega}(\mathcal{Z})$ is a projection operator that keeps the entries of \mathcal{Z} in Ω and sets all others to zero. Let

$$\Phi_{\mathbb{G}}(\mathcal{Z}) := \begin{cases} 0, & \text{if } \mathcal{Z} \in \mathbb{G}, \\ \infty, & \text{otherwise} \end{cases} \quad (3)$$

where $\mathbb{G} := \{\mathcal{Z} \in \mathbb{R}^{I_1 \times I_2 \times I_3}, P_{\Omega}(\mathcal{Z} - \mathcal{T}) = 0\}$.

It is not difficult to find that (1) and (2) are the problem of solving tensor rank minimization. As we all know, the most popular tensor recovery method is nuclear norm minimization. However, the definition of the rank of a tensor is not unique, different tensor rank and corresponding nuclear norm can be induced based on different tensor decomposition. The CANDECOMP/PARAFAC (CP) rank is equal to the smallest number of rank-1 tensors to achieve CP decomposition [21], but generally NP-hard to estimate accurately [22]. Another popular rank is the Tucker rank derived from the Tucker decomposition [23], which is defined as a vector whose i th element corresponds to the rank of the mode i unfolding matrix of tensor. Liu et al. [24] first proposed sum of nuclear norms (SNN) as a convex surrogate of Tucker rank, which significantly facilitated the development of the tensor recovery problem. But the SNN is not compact convex relaxation of Tucker rank, and this matrixing technique cannot fully exploit tensor structure information [25]. Furthermore, tensor tubal rank and multi-rank are obtained from tensor singular value decomposition (t-SVD) [26]. Since there is no need tensor matrixization in the calculation process, this allows better utilization of the tensor's internal structural information. Many multidimensional data in the real world can be well approximated by low-rank tensors, due to the fact that the singular values of the corresponding tensors are relatively

small, while a few large ones contain the main information. On this basis, the tensor nuclear norm (TNN) has been proposed as a convex relaxation of tubal-rank [27]. Recently, Zheng et al. [28] proposed a new form of rank (N-tubal rank) based on tubal rank, which adopts a new unfold method of higher-order tensors into third-order tensors in various directions. Benefiting from this, t-SVD can be applied to higher-order situations by solving third-order tensors of various directions forms. This approach not only enables t-SVD to be applied to higher order cases, but also makes good use of the properties of tensor tubal rank. In view of the excellent properties of N-tubal rank, we will use N-tubal rank to construct the model in this paper.

However, although nuclear norm relaxation is becoming a popular solution to the low rank tensor recovery problem, it still suffers from some drawbacks. TNN is a convex relaxation approximation of tensor tubal rank, and there is still a certain distance from tensor tubal rank minimization, which usually leads to the solution of the optimization problem being sub-optimal solution to the original problem. Recently, to break the limitation of biased estimation of convex relaxation methods, some non-convex relaxation strategies have been adopted to solve the tensor recovery problem. Non-convex methods are able to penalize larger singular values less and smaller singular values more. In [29], a t-Schatten-p norm was proposed to approximate tensor tubal rank by extending the Schatten-p norm. Another non-convex approach to approximating the tensor tubal rank is by transforming each element as a sum of t-TNNs with the Laplace function [30]. Besides, Logarithmic function [31], MCP function [32], [33], [34], SCAD function [35] are also applied to carry out non-convex relaxation. To further explore the superiority of non-convex functions and improve the accuracy of tensor recovery, we propose a new non-convex function in this paper, namely the Minimax Logarithmic Concave Penalty (MLCP) function. Interestingly, it is found that the Logarithmic function is an upper bound of the MLCP function. The proposed function is then generalized to higher dimensional cases, yielding vector MLCP, matrix MLCP, tensor MLCP, and weighted tensor $L\gamma$ -norm. However, when the proposed function is directly applied to the tensor recovery problem, the explicit solution cannot be obtained, which is very unfavorable to the solution of the algorithm. Therefore, we further put forward the corresponding equivalence theorems, namely vector equivalent MLCP theorem, matrix equivalent MLCP theorem, tensor equivalent MLCP theorem, and equivalent weighted tensor $L\gamma$ -norm theorem, to tackle this problem. Furthermore, we give the proximal operator for the equivalent weighted tensor $L\gamma$ -norm, which makes the tensor recovery model easier to solve. Finally, similar to the technique employed in [36], [37], [38], [39], using the Proximal Alternating Linearization Minimization Algorithm (PALM) [40], combined with the Kurdyka-Łojasiewicz property, we prove that the solution sequence obtained with MLCP functions has a finite length and converges globally to the critical point with stronger convergence.

In summary, the main contributions of our paper are:

First, a new non-convex function, Minimax Logarithmic Concave Penalty (MLCP) function, is proposed. It is found

that the Logarithmic function is an upper bound of the MLCP function. The function is generalized to tensor cases, yielding tensor MLCP and weighted tensor $L\gamma$ -norm. Considering that applying it directly to the tensor recovery problem, the explicit solution cannot be obtained, which is very unfavorable for the solution of the algorithm. For this reason, we give the corresponding equivalence theorems to solve this problem, namely tensor EMLCP, and equivalent weighted tensor $L\gamma$ -norm theorems. The properties of the tensor EMLCP and the equivalent weighted tensor $L\gamma$ -norm are analyzed. Furthermore, the proximal operator for the equivalent weighted tensor $L\gamma$ -norm is given, so as to make the tensor recovery model easier to solve.

Second, we construct corresponding EMLCP-based models for two typical problems of tensor recovery, and design a Proximal Alternating Linearization Minimization Algorithm (PALM) to solve these two EMLCP-based models. In particular, we adopt a model that removes mixed noise for the TRPCA problem, which is more realistic. Furthermore, based on the Kurdyka-Łojasiewicz property, it is proved that the solution sequence of the proposed algorithm has finite length and converges to the critical point globally.

Third, we conduct experiments on both LRTC and TRPCA using real data. The LRTC experiments on HSI, MRI, CV and the TRPCA experiments on HSI demonstrate the effectiveness of our proposed new non-convex relaxation method. This method yields better results than the Logarithmic relaxation method, which is consistent with our theoretical analysis.

The summary of this article is as follows: In Section II, some preliminary knowledge and background are given. The definitions and theorems of the MLCP function are presented in Section III. In Section IV, we establish the EMLCP-based models and algorithms. In Section V, we give the theoretical convergence analysis of the proposed algorithms. The results of extensive experiments and discussion are presented in Section VI. Conclusions are drawn in Section VII.

II. PRELIMINARIES

A. Tensor Notations and Definitions

In this section, we give some basic notations and briefly introduce some definitions used throughout the paper. Generally, a lowercase letter and an uppercase letter denote a vector z and a matrix Z , respectively. An N th-order tensor is denoted by a calligraphic upper case letter $\mathcal{Z} \in \mathbb{R}^{I_1 \times I_2 \times \dots \times I_N}$ and z_{i_1, i_2, \dots, i_N} is its (i_1, i_2, \dots, i_N) -th element. The Frobenius norm of a tensor is defined as $\|\mathcal{Z}\|_F = (\sum_{i_1, i_2, \dots, i_N} y_{i_1, i_2, \dots, i_N}^2)^{1/2}$. For a three order tensor $\mathcal{Z} \in \mathbb{R}^{I_1 \times I_2 \times I_3}$, we use $\tilde{\mathcal{Z}}$ to denote the discrete Fourier transformation (DFT) along each tubal of \mathcal{Z} , i.e., $\tilde{\mathcal{Z}} = \text{fft}(\mathcal{Z}, [], 3)$. The inverse DFT is computed by command ifft satisfying $\mathcal{Z} = \text{ifft}(\tilde{\mathcal{Z}}, [], 3)$. More often, the frontal slice $\mathcal{Z}(:, :, i)$ is denoted compactly as $\mathcal{Z}^{(i)}$.

Definition 1 (Mode- $k_1 k_2$ slices [28]): For an N th-order tensor $\mathcal{Z} \in \mathbb{R}^{I_1 \times I_2 \times \dots \times I_N}$, its mode- $k_1 k_2$ slices ($\mathcal{Z}^{(k_1 k_2)}$), $1 \leq k_1 < k_2 \leq N$, $k_1, k_2 \in \mathbb{Z}$ are two-dimensional sections, defined by fixing all but the mode- k_1 and the mode- k_2 indexes.

Definition 2 (Tensor Mode- k_1, k_2 Unfolding and Folding [28]): For an N th-order tensor $\mathcal{Z} \in \mathbb{R}^{I_1 \times I_2 \times \dots \times I_N}$, its mode- $k_1 k_2$ unfolding is a three order tensor denoted by $\mathcal{Z}_{(k_1 k_2)} \in$

$\mathbb{R}^{I_{k_1} \times I_{k_2} \times \prod_{s \neq k_1, k_2} I_s}$, the frontal slices of which are the lexicographic orderings of the mode- $k_1 k_2$ slices of \mathcal{Z} . Mathematically, the (i_1, i_2, \dots, i_N) -th element of \mathcal{Z} maps to the (i_{k_1}, i_{k_2}, j) -th element of $\mathcal{Z}_{(k_1 k_2)}$, where

$$j = 1 + \sum_{s=1, s \neq k_1, s \neq k_2}^N (i_s - 1) J_s \quad \text{with} \quad J_s = \prod_{m=1, m \neq k_1, m \neq k_2}^{s-1} I_m. \quad (4)$$

The mode- $k_1 k_2$ unfolding operator and its inverse operation are respectively denoted as $\mathcal{Z}_{(k_1 k_2)} := t - \text{unfold}(\mathcal{Z}, k_1, k_2)$ and $\mathcal{Z} := t - \text{fold}(\mathcal{Z}_{(k_1 k_2)}, k_1, k_2)$.

For a three order tensor $\mathcal{Z} \in \mathbb{R}^{I_1 \times I_2 \times I_3}$, the block circulation operation is defined as

$$\text{bcirc}(\mathcal{Z}) := \begin{pmatrix} \mathcal{Z}^{(1)} & \mathcal{Z}^{(I_3)} & \dots & \mathcal{Z}^{(2)} \\ \mathcal{Z}^{(2)} & \mathcal{Z}^{(1)} & \dots & \mathcal{Z}^{(3)} \\ \vdots & \vdots & \ddots & \vdots \\ \mathcal{Z}^{(I_3)} & \mathcal{Z}^{(I_3-1)} & \dots & \mathcal{Z}^{(1)} \end{pmatrix} \in \mathbb{R}^{I_1 I_3 \times I_2 I_3}.$$

The block diagonalization operation and its inverse operation are defined as

$$\text{bdiag}(\mathcal{Z}) := \begin{pmatrix} \mathcal{Z}^{(1)} & & & \\ & \mathcal{Z}^{(2)} & & \\ & & \ddots & \\ & & & \mathcal{Z}^{(I_3)} \end{pmatrix} \in \mathbb{R}^{I_1 I_3 \times I_2 I_3},$$

$$\text{bdfold}(\text{bdiag}(\mathcal{Z})) := \mathcal{Z}.$$

The block vectorization operation and its inverse operation are defined as

$$\text{bvec}(\mathcal{Z}) := \begin{pmatrix} \mathcal{Z}^{(1)} \\ \mathcal{Z}^{(2)} \\ \vdots \\ \mathcal{Z}^{(I_3)} \end{pmatrix} \in \mathbb{R}^{I_1 I_3 \times I_2}, \quad \text{bvfold}(\text{bvec}(\mathcal{Z})) := \mathcal{Z}.$$

Definition 3 (t-product [26]): Let $\mathcal{A} \in \mathbb{R}^{I_1 \times I_2 \times I_3}$ and $\mathcal{B} \in \mathbb{R}^{I_2 \times J \times I_3}$. Then the t-product $\mathcal{A} * \mathcal{B}$ is defined to be a tensor of size $I_1 \times J \times I_3$,

$$\mathcal{A} * \mathcal{B} := \text{bvfold}(\text{bcirc}(\mathcal{A}) \text{bvec}(\mathcal{B})).$$

Since that circular convolution in the spatial domain is equivalent to multiplication in the Fourier domain, the t-product between two tensors $\mathcal{C} = \mathcal{A} * \mathcal{B}$ is equivalent to

$$\bar{\mathcal{C}} = \text{bdfold}(\text{bdiag}(\bar{\mathcal{A}}) \text{bdiag}(\bar{\mathcal{B}})).$$

Definition 4 (Tensor conjugate transpose [26]): The conjugate transpose of a tensor $\mathcal{A} \in \mathbb{C}^{I_1 \times I_2 \times I_3}$ is the tensor $\mathcal{A}^H \in \mathbb{C}^{I_2 \times I_1 \times I_3}$ obtained by conjugate transposing each of the frontal slices and then reversing the order of transposed frontal slices 2 through I_3 .

Definition 5 (identity tensor [26]): The identity tensor $\mathcal{I} \in \mathbb{R}^{I_1 \times I_1 \times I_3}$ is the tensor whose first frontal slice is the $I_1 \times I_1$ identity matrix, and whose other frontal slices are all zeros.

It is clear that $\text{bcirc}(\mathcal{I})$ is the $I_1 I_3 \times I_1 I_3$ identity matrix. So it is easy to get $\mathcal{A} * \mathcal{I} = \mathcal{A}$ and $\mathcal{I} * \mathcal{A} = \mathcal{A}$.

Definition 6 (orthogonal tensor [26]): A tensor $\mathcal{Q} \in \mathbb{R}^{I_1 \times I_1 \times I_3}$ is orthogonal if it satisfies

$$\mathcal{Q} * \mathcal{Q}^H = \mathcal{Q}^H * \mathcal{Q} = \mathcal{I}.$$

Definition 7 (f-diagonal Tensor [26]): A tensor is called f-diagonal if each of its frontal slices is a diagonal matrix.

Theorem 1 (t-SVD [41]): Let $\mathcal{Z} \in \mathbb{R}^{I_1 \times I_2 \times I_3}$ be a three order tensor, then it can be factored as

$$\mathcal{Z} = \mathcal{U} * \mathcal{S} * \mathcal{V}^H,$$

where $\mathcal{U} \in \mathbb{R}^{I_1 \times I_1 \times I_3}$ and $\mathcal{V} \in \mathbb{R}^{I_2 \times I_2 \times I_3}$ are orthogonal tensors, and $\mathcal{S} \in \mathbb{R}^{I_1 \times I_2 \times I_3}$ is an f-diagonal tensor.

Definition 8 (tensor tubal-rank and multi-rank [42]): The tubal-rank of a tensor $\mathcal{Z} \in \mathbb{R}^{I_1 \times I_2 \times I_3}$, denoted as $\text{rank}_t(\mathcal{Z})$, is defined to be the number of non-zero singular tubes of \mathcal{S} , where \mathcal{S} comes from the t-SVD of $\mathcal{Z} : \mathcal{Z} = \mathcal{U} * \mathcal{S} * \mathcal{V}^H$. That is

$$\text{rank}_t(\mathcal{Z}) = \#\{i : \mathcal{S}(i, :, :) \neq 0\}. \quad (5)$$

The tensor multi-rank of $\mathcal{Z} \in \mathbb{R}^{I_1 \times I_2 \times I_3}$ is a vector, denoted as $\text{rank}_r(\mathcal{Z}) \in \mathbb{R}^{I_3}$, with the i -th element equals to the rank of i -th frontal slice of \mathcal{Z} .

Definition 9 (tensor nuclear norm (TNN)): The tensor nuclear norm of a tensor $\mathcal{Z} \in \mathbb{R}^{I_1 \times I_2 \times I_3}$, denoted as $\|\mathcal{Z}\|_{TNN}$, is defined as the sum of the singular values of all the frontal slices of $\bar{\mathcal{Z}}$, i.e.,

$$\|\mathcal{Z}\|_{TNN} := \sum_{i=1}^{I_3} \|\bar{\mathcal{Z}}^{(i)}\|_* \quad (6)$$

where $\bar{\mathcal{Z}}^{(i)}$ is the i -th frontal slice of $\bar{\mathcal{Z}}$, with $\bar{\mathcal{Z}} = \text{fft}(\mathcal{Z}, [], 3)$.

Definition 10 (N-tubal rank [28]): N-tubal rank of an Nth-order tensor $\mathcal{Y} \in \mathbb{R}^{I_1 \times I_2 \times \dots \times I_N}$ is defined as a vector, the elements of which contain the tubal rank of all mode- $k_1 k_2$ unfolding tensors, i.e.,

$$\begin{aligned} N - \text{rank}_t(\mathcal{Y}) := & (\text{rank}_t(\mathcal{Y}_{(12)}), \text{rank}_t(\mathcal{Y}_{(13)}), \dots, \\ & \text{rank}_t(\mathcal{Y}_{(1N)}), \text{rank}_t(\mathcal{Y}_{(23)}), \dots, \text{rank}_t(\mathcal{Y}_{(2N)}), \dots, \\ & \text{rank}_t(\mathcal{Y}_{(N-1N)})) \in \mathbb{R}^{N(N-1)/2}. \end{aligned} \quad (7)$$

Next, we will introduce some knowledge related to convergence analysis.

Definition 11 (Proper function [43]): Let \mathfrak{Y} be a finite-dimensional Euclidean space, a function $f : \mathfrak{Y} \rightarrow [-\infty, +\infty]$ is called proper if $f(z) < +\infty$ for at least one $z \in \mathfrak{Y}$, and $f(z) > -\infty$ for all $z \in \mathfrak{Y}$.

The effective domain of f is defined as $\text{dom}(f) := \{z : f(z) < +\infty\}$. For a given proper and lower semicontinuous function $f : \mathfrak{Y} \rightarrow (-\infty, +\infty]$, the proximal mapping associated with f at y is defined by

$$\text{Prox}_f(y) = \arg \min_{z \in \mathfrak{Y}} \{f(z) + \frac{1}{2} \|z - y\|^2\}, \quad \forall y \in \mathfrak{Y}.$$

Definition 12 (Subdifferential of a nonconvex function [43]): The subdifferential of $f : \mathbb{R}^n \rightarrow (-\infty, +\infty]$ at z , denoted as $\partial f(z)$, is defined by

$$\begin{aligned} \partial f(z) = & \{y \in \mathbb{R}^n : \exists z^k \rightarrow z, f(z^k) \rightarrow f(z), \\ & y^k \rightarrow y \text{ with } y^k \in \hat{\partial} f(z^k) \text{ as } k \rightarrow +\infty\}, \end{aligned}$$

where $\hat{\partial}f(z)$ denotes the Fréchet subdifferential of f at $z \in \text{dom}(f)$, which is the set of all y satisfying

$$\liminf_{x \rightarrow z, x \neq z} \frac{f(x) - f(z) - \langle y, x - z \rangle}{\|x - z\|} \geq 0. \quad (8)$$

For any $\mathcal{Z} \in \mathfrak{X}$, the distance from \mathcal{Z} to \mathfrak{Y} is defined by $\text{dist}(\mathcal{Z}, \mathfrak{Y}) := \inf\{\|\mathcal{Z} - \mathcal{Y}\|_F : \mathcal{Y} \in \mathfrak{Y}\}$, where \mathfrak{Y} is a subset of \mathfrak{X} . Next, we recall the Kurdyka–Łojasiewicz (KL) property, which plays a pivotal role in the analysis of the convergence of proximal alternating linearized minimization (PALM) algorithm for the nonconvex problems.

Definition 13 (KL function [40]): Let $f : \mathbb{R}^n \rightarrow (-\infty, +\infty]$ be a proper and lower semicontinuous function.

(a): The function f is said to have the KL property at $z \in \text{dom}(\partial f)$ if there exist $\eta \in (0, +\infty]$, a neighborhood \mathfrak{Y} of z and a continuous concave function $\phi : [0, \eta] \rightarrow [0, +\infty)$ such that: (a) $\phi(0) = 0$; (b) ϕ is continuously differentiable on $(0, \eta)$, and continuous at 0; (c) $\phi'(s) > 0$ for all $s \in (0, \eta)$; (d) for all $y \in \mathfrak{Y} \cap [y \in \mathbb{R}^n : f(z) < f(y) < f(z) + \eta]$, the following KL inequality holds:

$$\phi'(f(y) - f(z)) \text{dist}(0, \partial f(y)) \geq 1.$$

(b): If f satisfies the KL property at each point of $\text{dom}(\partial f)$, then f is called a KL function.

III. MINIMAX LOGARITHMIC CONCAVE PENALTY (MLCP) FUNCTION AND EQUIVALENT MINIMAX LOGARITHMIC CONCAVE PENALTY (EMLCP)

In this section, we first define the definition of the Minimax Logarithmic Concave Penalty (MLCP) function.

Definition 14 (Minimax Logarithmic Concave Penalty (MLCP) function): Let $\lambda > 0, \gamma > 0, \varepsilon > 0$. The MLCP function $f_{L,\gamma,\lambda} : \mathbb{R} \rightarrow \mathbb{R}_{\geq 0}$ is defined as

$$f_{L,\gamma,\lambda}(z) = \begin{cases} \lambda \log\left(\frac{|z|}{\varepsilon} + 1\right) - \frac{\log^2\left(\frac{|z|}{\varepsilon} + 1\right)}{2\gamma}, & |z| \leq \varepsilon e^{\gamma\lambda} - \varepsilon, \\ \frac{\gamma\lambda^2}{2}, & |z| > \varepsilon e^{\gamma\lambda} - \varepsilon. \end{cases} \quad (9)$$

The MLCP function is a symmetric function, so we only discuss its functional properties on $[0, +\infty)$.

Proposition 1: The MLCP function defined in (9) satisfies the following properties:

(a): $f_{L,\gamma,\lambda}(z)$ is continuous, smooth and

$$f_{L,\gamma,\lambda}(0) = 0, \lim_{z \rightarrow +\infty} \frac{f_{L,\gamma,\lambda}(z)}{z} = 0;$$

(b): $f_{L,\gamma,\lambda}(z)$ is monotonically non-decreasing and concave on $[0, +\infty)$;

(c): $f'_{L,\gamma,\lambda}(z)$ is non-negativity and monotonicity non-increasing on $[0, +\infty)$. Moreover, it is Lipschitz bounded, i.e., there exists constant $L(f)$ such that

$$|f'_{L,\gamma,\lambda}(x) - f'_{L,\gamma,\lambda}(y)| \leq L(f)|x - y|;$$

(d): Especially, for the MLCP function, it is increasing in parameter γ , and

$$\lim_{\gamma \rightarrow +\infty} f_{L,\gamma,\lambda}(z) = \lambda \log\left(\frac{|z|}{\varepsilon} + 1\right). \quad (10)$$

Proof: The proof is provided in Appendix A. ■

Definition 15 (Vector MLCP): Let $z \in \mathbb{R}^n$ and $\lambda > 0, \gamma > 0, \varepsilon > 0$. The vector MLCP $f_{L,\gamma,\lambda} : \mathbb{R}^n \rightarrow \mathbb{R}_{\geq 0}$ is defined as

$$f_{L,\gamma,\lambda}(z) = \sum_{i=1}^n f_{L,\gamma,\lambda}(z_i), \quad (11)$$

where z_i denotes the i th entry of the vector z and $f_{L,\gamma,\lambda}(z_i)$ is defined in (9).

Definition 16 (Matrix MLCP): Let $Z \in \mathbb{R}^{m \times n}$ and $\lambda > 0, \gamma > 0, \varepsilon > 0$. The matrix MLCP $f_{L,\gamma,\lambda} : \mathbb{R}^{m \times n} \rightarrow \mathbb{R}_{\geq 0}$ is defined as

$$f_{L,\gamma,\lambda}(Z) = \sum_{i=1}^m \sum_{j=1}^n f_{L,\gamma,\lambda}(Z_{ij}), \quad (12)$$

where Z_{ij} denotes the (i, j) element of Z , and $f_{L,\gamma,\lambda}$ is the same as in (9).

Definition 17 (Tensor MLCP): Let $\mathcal{Z} \in \mathbb{R}^{I_1 \times I_2 \times \dots \times I_N}$ and $\bar{\lambda} > 0, \gamma > 0, \varepsilon > 0, \bar{\lambda} \in \mathbb{R}^{I_1 \times I_2 \times \dots \times I_N}$. The tensor MLCP $f_{L,\gamma,\bar{\lambda}} : \mathbb{R}^{I_1 \times I_2 \times \dots \times I_N} \rightarrow \mathbb{R}_{\geq 0}$ is defined as

$$f_{L,\gamma,\bar{\lambda}}(\mathcal{Z}) = \sum_{i_1=1}^{I_1} \sum_{i_2=1}^{I_2} \dots \sum_{i_N=1}^{I_N} f_{L,\gamma,\bar{\lambda}_{i_1, i_2, \dots, i_N}}(\mathcal{Z}_{i_1, i_2, \dots, i_N}), \quad (13)$$

where $\mathcal{Y}_{i_1, i_2, \dots, i_N}$ denotes the (i_1, i_2, \dots, i_N) -th element of \mathcal{Y} , and $h_{\gamma,\bar{\lambda}}$ is defined in (9).

Definition 18 (Matrix $L\gamma$ -norm): The $L\gamma$ norm of a rank- r matrix $Z \in \mathbb{R}^{m \times n}$, denoted by $\|Z\|_{L,\gamma,\lambda}$, is defined in terms of the singular values $\{\sigma_i, i = 1, 2, \dots, r\}$ as follows:

$$\|Z\|_{L,\gamma,\lambda} := f_{L,\gamma,\lambda}(\sigma) = \sum_{i=1}^r f_{L,\gamma,\lambda}(\sigma_i), \quad (14)$$

where σ is singular value vector of matrix Z .

Similarly, the weighted matrix $L\gamma$ -norm is a generalization of weighted MLCP for matrix and is defined as follows.

Definition 19 (Weighted matrix $L\gamma$ -norm): The weighted matrix $L\gamma$ -norm of $Z \in \mathbb{R}^{m \times n}$, denoted by $\|Z\|_{L,\gamma,\lambda}$, is defined as follows:

$$\|Z\|_{L,\gamma,\lambda} = f_{L,\gamma,\lambda}(\sigma) = \sum_{i=1}^r f_{L,\gamma,\lambda_i}(\sigma_i). \quad (15)$$

where $r = \min(m, n)$ denotes the maximum rank of Z .

Definition 20 (Weighted tensor $L\gamma$ -norm): The weighted tensor $L\gamma$ -norm of $\mathcal{Z} \in \mathbb{R}^{I_1 \times I_2 \times I_3}$, denoted by $\|\mathcal{Z}\|_{L,\gamma,\bar{\lambda}}$, is defined as follows:

$$\|\mathcal{Z}\|_{L,\gamma,\bar{\lambda}} = \sum_{i=1}^{I_3} \|\bar{\mathcal{Z}}^{(i)}\|_{L,\gamma,\bar{\lambda}_i} = \sum_{i=1}^{I_3} \sum_{j=1}^R f_{L,\gamma,\bar{\lambda}_{i,j}}(\sigma_j(\bar{\mathcal{Z}}^{(i)})). \quad (16)$$

where $R = \min(I_1, I_2)$.

Further, we convert λ from a constant to a variable, for which we propose some equivalent MLCP theorems.

Theorem 2 (Scalar EMLCP): Let $\lambda > 0, \gamma > 0, \varepsilon > 0$ and $z \in \mathbb{R}$. The scalar MLCP $f_{L,\gamma,\lambda} : \mathbb{R} \rightarrow \mathbb{R}_{\geq 0}$ is the solution of the following optimization problem:

$$f_{L,\gamma,\lambda}(z) = \min_{\omega \in \mathbb{R}_{\geq 0}} \left\{ \omega \log\left(\frac{|z|}{\varepsilon} + 1\right) + \frac{\gamma}{2}(\omega - \lambda)^2 \right\}. \quad (17)$$

Proof: The proof is provided in Appendix B. ■

Theorem 3 (Vector EMLCP): Let $\gamma > 0, \varepsilon > 0, \omega \in \mathbb{R}_{\geq 0}^n, \lambda \in \mathbb{R}_{\geq 0}^n$ and $z \in \mathbb{R}^n$. The vector MCP is the solution of the following optimization problem:

$$f_{L,\gamma,\lambda}(z) = \min_{\omega \in \mathbb{R}_{\geq 0}^n} \{ \|z\|_{L,\omega} + \frac{\gamma}{2} \|\omega - \lambda\|_2^2 \}, \quad (18)$$

where $\|z\|_{L,\omega}$ is defined as

$$\|z\|_{L,\omega} = \sum_{i=1}^n \omega_i \log\left(\frac{|z_i|}{\varepsilon} + 1\right), \omega_i \geq 0,$$

and $\{\omega_i, i = 1, 2, \dots, n\}$ denote the weights.

Proof: The proof is provided in Appendix C. ■

Theorem 4 (Matrix EMLCP): Let $\gamma > 0, \varepsilon > 0, \Omega \in \mathbb{R}_{\geq 0}^{m \times n}, \Lambda \in \mathbb{R}_{\geq 0}^{m \times n}$ and $Z \in \mathbb{R}^{m \times n}$. The matrix MLCP is the solution of the following optimization problem:

$$f_{L,\gamma,\Lambda}(Z) = \min_{\Omega \in \mathbb{R}_{\geq 0}^{m \times n}} \{ \|Z\|_{L,\Omega} + \frac{\gamma}{2} \|\Omega - \Lambda\|_2^2 \}, \quad (19)$$

where $\|Z\|_{L,\Omega}$ is defined as

$$\|Z\|_{L,\Omega} = \sum_{i=1}^m \sum_{j=1}^n \Omega_{ij} \log\left(\frac{|Z_{ij}|}{\varepsilon} + 1\right),$$

where $\{\Omega_{ij} \geq 0, i = 1, 2, \dots, m, j = 1, 2, \dots, n\}$ denote the weights.

Proof: The proof is provided in Appendix D. ■

Theorem 5 (Tensor EMLCP): Let $\gamma > 0, \varepsilon > 0, \mathcal{W}, \bar{\lambda} \in \mathbb{R}_{\geq 0}^{I_1 \times I_2 \times \dots \times I_N}$ and $\mathcal{Z} \in \mathbb{R}^{I_1 \times I_2 \times \dots \times I_N}$. The tensor MLCP is the solution to the optimization problem:

$$f_{L,\gamma,\bar{\lambda}}(\mathcal{Z}) = \min_{\mathcal{W}} \{ \|\mathcal{Z}\|_{L,\mathcal{W}} + \frac{\gamma}{2} \|\mathcal{W} - \bar{\lambda}\|_F^2 \}, \quad (20)$$

where $\|\mathcal{Z}\|_{L,\mathcal{W}}$ is defined as

$$\|\mathcal{Z}\|_{L,\mathcal{W}} = \sum_{i_1=1}^{I_1} \sum_{i_2=1}^{I_2} \dots \sum_{i_N=1}^{I_N} \mathcal{W}_t \log\left(\frac{|\mathcal{Z}_t|}{\varepsilon} + 1\right), \quad (21)$$

where \mathcal{W} is weight tensor, and $t = i_1, i_2, \dots, i_N$.

Proof: The proof is provided in Appendix E. ■

Remark 1: As the order of the tensor decreases, tensor EMLCP can degenerate into the form of matrix EMLCP, vector EMLCP, and scalar EMLCP respectively.

Theorem 6 (Equivalent weighted matrix $L\gamma$ -norm): Consider a rank- r matrix $Z \in \mathbb{R}^{m \times n}$ with the SVD: $Z = U \text{diag}(\sigma) V^T$, where $\sigma = [\sigma_1, \sigma_2, \dots, \sigma_r]^T$. Let $\Omega, \Lambda \in \mathbb{R}_{\geq 0}^r$, and $\gamma > 0, \varepsilon > 0$. The matrix $L\gamma$ -norm is obtained equivalently as

$$\|Z\|_{L,\gamma,\Lambda} = \min_{\Omega} \{ \|Z\|_{L,\Omega} + \frac{\gamma}{2} \|\Omega - \Lambda\|_2^2 \}, \quad (22)$$

where $\|Z\|_{L,\Omega} = \sum_{i=1}^r \Omega_i \log\left(\frac{\sigma_i}{\varepsilon} + 1\right)$.

Proof: The proof is provided in Appendix F. ■

Theorem 7 (Equivalent weighted Tensor $L\gamma$ -norm): For a third-order tensor $\mathcal{Z} \in \mathbb{R}^{I_1 \times I_2 \times I_3}$, its SVD is decomposed into $\mathcal{Z} = \mathcal{U} * \mathcal{S} * \mathcal{V}$, where $\mathcal{S} \in \mathbb{R}^{R \times R \times I_3}$ and $R = \min\{I_1, I_2\}$. Let $W, \bar{\Lambda} \in \mathbb{R}_{\geq 0}^{R \times I_3}$, and $\gamma > 0, \varepsilon > 0$. The weighted tensor $L\gamma$ -norm is obtained equivalently as

$$\|\mathcal{Z}\|_{L,\gamma,\bar{\Lambda}} = \min_{W} \{ \|\mathcal{Z}\|_{L,W} + \frac{\gamma}{2} \|W - \bar{\Lambda}\|_F^2 \}, \quad (23)$$

where

$$\begin{aligned} \|\mathcal{Z}\|_{L,W} &:= \sum_{i_3=1}^{I_3} \|\bar{\mathcal{Z}}^{(i_3)}\|_{L,W_{(\cdot,i_3)}} \\ &= \sum_{j=1}^R W_{j,i_3} \log\left(\frac{\sigma_j(\bar{\mathcal{Z}}^{(i_3)})}{\varepsilon} + 1\right). \end{aligned}$$

Proof: The proof is provided in Appendix G. ■

Remark 2: In particular, when the third dimension I_3 of the third-order tensor \mathcal{Z} is 1, equivalent weighted Tensor $L\gamma$ -norm can degenerate into the form of equivalent weighted matrix $L\gamma$ -norm.

Remark 3: Unlike the l_1 penalty or the nuclear norm penalty, the tensor MLCP (13), tensor EMLCP (20), weighted tensor $L\gamma$ -norm (16), and equivalent weighted tensor $L\gamma$ -norm (23) do not satisfy the triangle inequality. Some vital properties of the tensor EMLCP and equivalent weighted tensor $L\gamma$ -norm are given below.

Proposition 2: The tensor EMLCP $f_{L,\gamma,\bar{\lambda}}(\mathcal{Z})$ is defined in (20) satisfies the following properties:

(a) **Non-negativity:** The tensor EMLCP is non-negative, i.e., $f_{L,\gamma,\bar{\lambda}}(\mathcal{Z}) \geq 0$. The equality holds if and only if \mathcal{Z} is the null tensor.

(b) **Concavity:** $f_{L,\gamma,\bar{\lambda}}(\mathcal{Z})$ is concave in the modulus of the elements of \mathcal{Z} .

(c) **Boundedness:** The tensor EMLCP is upper-bounded by the weighted Logarithmic norm, i.e., $f_{L,\gamma,\bar{\lambda}}(\mathcal{Z}) \leq \|\mathcal{Z}\|_{L,W}$.

(d) **Asymptotic l_1 property:** The tensor EMLCP approaches the weighted Logarithmic norm asymptotically, i.e., $\lim_{\gamma \rightarrow \infty} f_{L,\gamma,\bar{\lambda}}(\mathcal{Z}) = \|\mathcal{Z}\|_{L,W}$

Proof: The proof is provided in Appendix H. ■

Proposition 3: The equivalent weighted tensor $L\gamma$ -norm is defined in (23) satisfies the following properties:

(a) **Non-negativity:** The equivalent weighted tensor $L\gamma$ -norm is non-negative, i.e., $\|\mathcal{Z}\|_{L,\gamma,\bar{\Lambda}} \geq 0$. The equality holds if and only if \mathcal{Z} is the null tensor.

(b) **Concavity:** $\|\mathcal{Z}\|_{L,\gamma,\bar{\Lambda}}$ is concave in the modulus of the elements of \mathcal{Z} .

(c) **Boundedness:** The equivalent weighted tensor $L\gamma$ -norm is upper-bounded by the weighted Logarithmic norm, i.e., $\|\mathcal{Z}\|_{L,\gamma,\bar{\Lambda}} \leq \|\mathcal{Z}\|_{L,W}$.

(d) **Asymptotic nuclear norm property:** The equivalent weighted tensor $L\gamma$ -norm approaches the weighted Logarithmic norm asymptotically, i.e., $\lim_{\gamma \rightarrow \infty} \|\mathcal{Z}\|_{L,\gamma,\bar{\Lambda}} = \|\mathcal{Z}\|_{L,W}$.

(e) **Unitary invariance:** The equivalent weighted tensor $L\gamma$ -norm is unitary invariant, i.e., $\|\mathcal{U} * \mathcal{Z} * \mathcal{V}\|_{L,\gamma,\bar{\Lambda}} = \|\mathcal{Z}\|_{L,\gamma,\bar{\Lambda}}$, for unitary tensor \mathcal{U} and \mathcal{V} .

Proof: The proof is provided in Appendix I. ■

Theorem 8 (Proximal operator for equivalent weighted tensor $L\gamma$ -norm): Consider equivalent weighted tensor $L\gamma$ -norm given in (23). Its proximal operator denoted by $S_{L,\gamma,\bar{\Lambda}} : \mathbb{R}^{I_1 \times I_2 \times I_3} \rightarrow \mathbb{R}^{I_1 \times I_2 \times I_3}$, $W, \bar{\Lambda} \in \mathbb{R}_{\geq 0}^{R \times I_3}$, and $\gamma > 0, \varepsilon > 0$, $R = \min\{I_1, I_2\}$ and defined as follows:

$$S_{L,\gamma,\bar{\Lambda}}(\mathcal{Y}) = \arg \min_{\mathcal{L}} \left\{ \frac{\rho}{2} \|\mathcal{L} - \mathcal{Y}\|_F^2 + \|\mathcal{L}\|_{L,\gamma,\bar{\Lambda}} \right\}, \quad (24)$$

Algorithm 1 EMLCPTC

Input: An incomplete tensor \mathcal{T} , the index set of the known elements Ω , convergence criteria ϵ , maximum iteration number K .

Initialization: $\mathcal{Z}^0 = \mathcal{T}_\Omega$, $M_{k_1 k_2}^0 = \mathcal{X}^0$, $\mu_{k_1 k_2}^0 > 0$, $\rho > 0, \tau > 1$.

- 1: **while** not converged and $k < K$ **do**
- 2: Updating $W_{k_1 k_2}^k$ via (32);
- 3: Updating $M_{k_1 k_2}^k$ via (33);
- 4: Updating \mathcal{Z}^k via (36);
- 5: Updating the multipliers $Q_{k_1 k_2}^k$ via (37);
- 6: $\mu_{k_1 k_2}^k = \tau \mu_{k_1 k_2}^{k-1}$, $\rho = \tau \rho$ $k = k + 1$;
- 7: Check the convergence conditions $\|\mathcal{Z}^{k+1} - \mathcal{Z}^k\|_\infty \leq \epsilon$.
- 8: **end while**
- 9: **return** \mathcal{Z}^{k+1} .

Output: Completed tensor $\mathcal{Z} = \mathcal{Z}^{k+1}$.

is given by

$$S_{L,\gamma,\bar{\Lambda}} = \begin{cases} W_{j,i} = \max\{\bar{\Lambda}_{j,i} - \frac{\log(\frac{\sigma_j(\bar{\mathcal{L}}^{(i)})}{\epsilon} + 1)}{\gamma}, 0\}, \\ \mathcal{L} = \mathcal{U} * \mathcal{S}_1 * \mathcal{V}^H, \end{cases} \quad (25)$$

where \mathcal{U} and \mathcal{V} are derived from the t-SVD of $\mathcal{Y} = \mathcal{U} * \mathcal{S}_2 * \mathcal{V}^H$. More importantly, the i th front slice of DFT of \mathcal{S}_1 and \mathcal{S}_2 , i.e., $\bar{\mathcal{S}}_1^{(i)} = \sigma(\bar{\mathcal{L}}^{(i)})$ and $\bar{\mathcal{S}}_2^{(i)} = \sigma(\bar{\mathcal{Y}}^{(i)})$, has the following relationship

$$\sigma_j(\bar{\mathcal{L}}^{(i)}) = \begin{cases} 0, & \text{if } \sigma_j(\bar{\mathcal{Y}}^{(i)}) \leq 2\sqrt{\alpha} - \epsilon, \\ \frac{l_1 + l_2}{2}, & \text{if } \sigma_j(\bar{\mathcal{Y}}^{(i)}) > 2\sqrt{\alpha} - \epsilon, \end{cases} \quad (26)$$

where $l_1 = \sigma_j(\bar{\mathcal{Y}}^{(i)}) - \epsilon$, $l_2 = \sqrt{(\sigma_j(\bar{\mathcal{Y}}^{(i)}) + \epsilon)^2 - 4\alpha}$, $\alpha = \frac{W_{j,i}}{\rho}$.

Proof: The proof is provided in Appendix J. \blacksquare

IV. EMLCP-BASED MODELS AND SOLVING ALGORITHMS

In this section, we apply the EMLCP to low rank tensor completion (LRTC) and tensor robust principal component analysis (TRPCA) and propose the EMLCP-based models with proximal alternating linearized minimization algorithms.

A. EMLCP-based LRTC model

Tensor completion aims at estimating the missing elements from an incomplete observation tensor. Considering an N -order tensor $\mathcal{Z} \in \mathbb{R}^{I_1 \times I_2 \times \dots \times I_N}$, the proposed EMLCP-based LRTC model is formulated as follow

$$\min_{\mathcal{Z}, W} \sum_{1 \leq k_1 < k_2 \leq N} \beta_{k_1 k_2} (\|\mathcal{Z}_{(k_1 k_2)}\|_{L,W} + \frac{\gamma}{2} \|W_{(k_1 k_2)} - \bar{\Lambda}\|_F^2) + \Phi_{\mathbb{G}}(\mathcal{Z}) \quad (27)$$

where \mathcal{Z} is the reconstructed tensor and \mathcal{T} is the observed tensor, Ω is the index set for the known entries, and $\mathcal{P}_\Omega(\mathcal{Z})$ is a projection operator that keeps the entries of \mathcal{Z} in Ω and sets all others to zero, $\beta_{k_1 k_2} \geq 0$ ($1 \leq k_1 < k_2 \leq N$, $k_1, k_2 \in \mathbb{Z}$) and $\sum_{1 \leq k_1 < k_2 \leq N} \beta_{k_1 k_2} = 1$. Let

$$\Phi_{\mathbb{G}}(\mathcal{Z}) := \begin{cases} 0, & \text{if } \mathcal{Z} \in \mathbb{G}, \\ \infty, & \text{otherwise} \end{cases} \quad (28)$$

where $\mathbb{G} := \{\mathcal{Z} \in \mathbb{R}^{I_1 \times I_2 \times \dots \times I_N}, \mathcal{P}_\Omega(\mathcal{Z} - \mathcal{T}) = 0\}$.

Next, we exploit the PALM to solve (27). We first introduce auxiliary variables $\mathcal{M}_{k_1 k_2}$, and then rewrite (27) as the following equivalent constrained problem:

$$\min_{\mathcal{Z}, W} \sum_{1 \leq k_1 < k_2 \leq N} \beta_{k_1 k_2} (\|\mathcal{M}_{(k_1 k_2)}\|_{L,W} + \frac{\gamma}{2} \|W_{(k_1 k_2)} - \bar{\Lambda}\|_F^2) + \Phi_{\mathbb{G}}(\mathcal{Z}) \quad (29)$$

s.t. $\mathcal{Z} = \mathcal{M}_{k_1 k_2}, 1 \leq k_1 < k_2 \leq N, k_1, k_2 \in \mathbb{Z}$.

The augmented Lagrangian function of (29) can be expressed in the following concise form:

$$\begin{aligned} LAG(\mathcal{Z}, \mathcal{M}, W, \bar{\Lambda}, \mathcal{Q}) &= \sum_{1 \leq k_1 < k_2 \leq N} \beta_{k_1 k_2} (\|\mathcal{M}_{(k_1 k_2)}\|_{L,W} + \frac{\gamma}{2} \|W_{(k_1 k_2)} - \bar{\Lambda}\|_F^2) \\ &+ \Phi_{\mathbb{G}}(\mathcal{Z}) + \frac{\mu_{k_1 k_2}}{2} \|\mathcal{Z} - \mathcal{M}_{k_1 k_2} + \frac{\mathcal{Q}_{k_1 k_2}}{\mu_{k_1 k_2}}\|_F^2, \\ &= H_1(\mathcal{M}, W) + H_2(W, \bar{\Lambda}) + \Phi_{\mathbb{G}}(\mathcal{Z}) + H_3(\mathcal{M}, \mathcal{Z}), \end{aligned} \quad (30)$$

where $\mathcal{Q}_{k_1 k_2}$ ($1 \leq k_1 \leq k_2 \leq N$) are the Lagrange multipliers, $\mu_{k_1 k_2}$ are positive scalars. For the sake of convenience, we denote the variable updated by the iteration as $(\cdot)^+$, the last iteration result as $(\cdot)^*$, and omit the specific number of iterations. With the proximal linearization of each subproblem, the PALM algorithm on the four blocks $(\mathcal{Z}, \mathcal{M}, W, \bar{\Lambda})$ for solving (29) yields the iteration scheme alternatingly as follows:

$$\begin{cases} W^+ = \min_W H_1(W) + H_2(W) + \frac{\rho^*}{2} \|W - W^*\|_F^2, \\ \mathcal{M}^+ = \min_{\mathcal{M}} H_1(\mathcal{M}) + \langle \mathcal{M} - \mathcal{M}^*, \nabla H_3(\mathcal{M}^*) \rangle \\ + \frac{\rho^*}{2} \|\mathcal{M} - \mathcal{M}^*\|_F^2, \\ \bar{\Lambda}^+ = \min_{\bar{\Lambda}} H_2(\bar{\Lambda}) + \frac{\rho^*}{2} \|\bar{\Lambda} - \bar{\Lambda}^*\|_F^2, \\ \mathcal{Z}^+ = \min_{\mathcal{Z}} \Phi_{\mathbb{G}}(\mathcal{Z}) + H_3(\mathcal{Z}) + \frac{\rho^*}{2} \|\mathcal{Z} - \mathcal{Z}^*\|_F^2, \end{cases} \quad (31)$$

From Theorem 8, the updates of W and \mathcal{M} are as follows:

$$W_{j,i}^+ = \max\left(\frac{\gamma \bar{\Lambda}_{j,i}^* + \rho^* W_{j,i}^* - \log(\frac{\sigma_j(\mathcal{M}^{*(i)})}{\epsilon} + 1)}{\gamma + \rho^*}, 0\right), \quad (32)$$

$$\mathcal{M}^+ = \mathcal{U} * \mathcal{S}_1 * \mathcal{V}^H, \quad (33)$$

where \mathcal{U} and \mathcal{V} are derived from the t-SVD of $\mathcal{M}^* + \frac{\mu \mathcal{Z}^* + \mathcal{Q}^* - \mu \mathcal{M}^*}{\rho^*} = \mathcal{U} * \mathcal{S}_2 * \mathcal{V}^H$. The relationship between \mathcal{S}_1 and \mathcal{S}_2 is given by Theorem 8.

The update for $\bar{\Lambda}$ turns out to be straightforward:

$$\begin{aligned} \bar{\Lambda}^+ &= \min_{\bar{\Lambda}} \frac{\gamma}{2} \|W^+ - \bar{\Lambda}\|_F^2 + \frac{\rho^*}{2} \|\bar{\Lambda} - \bar{\Lambda}^*\|_F^2 \\ &= \frac{\gamma W^+ + \rho^* \bar{\Lambda}^*}{\gamma + \rho^*}. \end{aligned} \quad (34)$$

Fixed $W_{k_1 k_2}$, $\mathcal{M}_{k_1 k_2}$, $\bar{\Lambda}_{k_1 k_2}$ and $\mathcal{Q}_{k_1 k_2}$, the minimization problem of \mathcal{Z} is as follows:

$$\min_{\mathcal{Z}} \sum_{1 \leq k_1 < k_2 \leq N} \frac{\mu_{k_1 k_2}}{2} \|\mathcal{Z} - \mathcal{M}_{k_1 k_2}^+ + \frac{\mathcal{Q}_{k_1 k_2}^*}{\mu_{k_1 k_2}}\|_F^2 + \Phi_{\mathbb{G}}(\mathcal{Z}) + \frac{\rho^*}{2} \|\mathcal{Z} - \mathcal{Z}^*\|_F^2. \quad (35)$$

The closed form of \mathcal{Z} can be derived by setting the derivative of (35) to zero. We can now update \mathcal{Z} by the following equation:

$$\mathcal{Z}^+ = \mathcal{P}_\Omega(\mathcal{T}) + \mathcal{P}_{\Omega^c} \left(\frac{\sum_{1 \leq k_1 < k_2 \leq N} \mu_{k_1 k_2} \mathcal{M}_{k_1 k_2}^* - \mathcal{Q}_{k_1 k_2}^* + \rho^* \mathcal{Z}^*}{\sum_{1 \leq k_1 < k_2 \leq N} \mu_{k_1 k_2} + \rho^*} \right). \quad (36)$$

Finally, multipliers $\mathcal{Q}_{k_1 k_2}$ are updated as follows:

$$\mathcal{Q}_{k_1 k_2}^+ = \mathcal{Q}_{k_1 k_2}^* + \mu_{k_1 k_2} (\mathcal{Z}^+ - \mathcal{M}_{k_1 k_2}^+). \quad (37)$$

The EMLCP-based LRTC model computation is given in Algorithm 1. The main per-iteration cost lies in the update of $\mathcal{M}_{k_1 k_2}$, which requires computing t-SVD. The per-iteration complexity is $O(LE(\sum_{1 \leq k_1 < k_2 \leq N} [\log(le_{k_1 k_2}) + \min(I_{k_1}, I_{k_2})]))$, where $LE = \prod_{i=1}^N I_i$ and $le_{k_1 k_2} = LE / (I_{k_1} I_{k_2})$.

B. EMLCP-based TRPCA model

Tensor robust PCA (TRPCA) aims to recover the tensor from grossly corrupted observations. Using the proposed EMLCP, we can get the following EMLCP-based TRPCA model:

$$\min_{\mathcal{L}, \mathcal{E}, \mathcal{N}} \sum_{1 \leq k_1 < k_2 \leq N} \beta_{k_1 k_2} (\|\mathcal{L}_{(k_1 k_2)}\|_{L, W} + \frac{\gamma}{2} \|W_{(k_1 k_2)} - \bar{\Lambda}\|_F^2) + \tau_1 \|\mathcal{E}\|_1 + \tau_2 \|\mathcal{N}\|_F \quad s.t. \quad \mathcal{T} = \mathcal{L} + \mathcal{E} + \mathcal{N}, \quad (38)$$

where \mathcal{T} is the corrupted observation tensor, \mathcal{L} is the low-rank component, \mathcal{E} is the sparse noise component, \mathcal{N} is the Gaussian noise component, and τ_1, τ_2 are tuning parameters compromising \mathcal{L} , \mathcal{E} and \mathcal{N} . Similarly, we introduce auxiliary variables $\mathcal{G}_{k_1 k_2}$, and then rewrite (38) as the following equivalent constrained problem:

$$\min_{\mathcal{L}, \mathcal{E}, \mathcal{N}} \sum_{1 \leq k_1 < k_2 \leq N} \beta_{k_1 k_2} (\|\mathcal{G}_{(k_1 k_2)}\|_{L, W} + \frac{\gamma}{2} \|W_{(k_1 k_2)} - \bar{\Lambda}\|_F^2) + \tau_1 \|\mathcal{E}\|_1 + \tau_2 \|\mathcal{N}\|_F \quad s.t. \quad \mathcal{T} = \mathcal{L} + \mathcal{E} + \mathcal{N}, \quad \mathcal{L} = \mathcal{G}_{k_1 k_2}, 1 \leq k_1 < k_2 \leq N, k_1, k_2 \in \mathbb{Z}. \quad (39)$$

The augmented Lagrangian function of (39) can be expressed in the following concrete form:

$$\begin{aligned} LAG(\mathcal{L}, \mathcal{G}, W, \bar{\Lambda}, \mathcal{R}, \mathcal{E}, \mathcal{N}, \mathcal{F}) &= \\ &\sum_{1 \leq k_1 < k_2 \leq N} \beta_{k_1 k_2} (\|\mathcal{G}_{(k_1 k_2)}\|_{L, W} + \frac{\gamma}{2} \|W_{(k_1 k_2)} - \bar{\Lambda}\|_F^2) \\ &+ \tau_1 \|\mathcal{E}\|_1 + \tau_2 \|\mathcal{N}\|_F + \frac{\mu_{k_1 k_2}}{2} \|\mathcal{L} - \mathcal{G}_{k_1 k_2}\|_F^2 + \frac{\mathcal{R}_{k_1 k_2}}{\mu_{k_1 k_2}} \|\mathcal{F}\|_F^2 \\ &+ \frac{\tau}{2} \|\mathcal{T} - \mathcal{L} - \mathcal{E} - \mathcal{N} + \frac{\mathcal{F}}{\tau}\|_F^2 \\ &= H_1(\mathcal{G}, W) + H_2(W, \bar{\Lambda}) + H_3(\mathcal{E}) \\ &+ H_4(\mathcal{N}) + H_5(\mathcal{L}, \mathcal{G}) + H_6(\mathcal{L}, \mathcal{E}, \mathcal{N}) \end{aligned} \quad (40)$$

where \mathcal{F} and $R_{k_1 k_2}$ ($1 \leq k_1 < k_2 \leq N$) are the Lagrange multipliers, $\mu_{k_1 k_2}$, τ_1 , τ_2 and τ are positive scalars. Similar to EMLCP-based LRTC model, we denote the variable updated by the iteration as $(\cdot)^+$, the last iteration result as $(\cdot)^*$, and omit the specific number of iterations. With the proximal linearization of each subproblem, the PALM algorithm on

Algorithm 2 EMLCPTPRCA

Input: The corrupted observation tensor \mathcal{T} , convergence criteria ϵ , maximum iteration number K .

Initialization: $\mathcal{L}^0 = \mathcal{T}$, $\mathcal{G}_{k_1 k_2}^0 = \mathcal{L}^0$, $\mu_{k_1 k_2}^0 > 0$, $\rho^0 > 0$, $\tau^0 > 0$, $\nu > 1$.

- 1: **while** not converged and $k < K$ **do**
- 2: Updating $W_{k_1 k_2}^k$ via (42);
- 3: Updating $\mathcal{G}_{k_1 k_2}^k$ via (43);
- 4: Updating $\bar{\Lambda}_{k_1 k_2}^k$ via (44);
- 5: Updating \mathcal{L}^k via (46);
- 6: Updating \mathcal{E}^k via (48);
- 7: Updating \mathcal{N}^k via (50);
- 8: Updating the multipliers $\mathcal{R}_{k_1 k_2}^k$ and \mathcal{F}^k via (51);
- 9: $\mu_{k_1 k_2}^k = \nu \mu_{k_1 k_2}^{k-1}$, $\rho^k = \nu \rho^{k-1}$, $\tau^k = \nu \tau^{k-1}$ $k = k + 1$;
- 10: Check the convergence conditions $\|\mathcal{L}^{k+1} - \mathcal{L}^k\|_\infty \leq \epsilon$.
- 11: **end while**
- 12: **return** \mathcal{L}^{k+1} , \mathcal{E}^{k+1} and \mathcal{N}^{k+1} .

Output: \mathcal{L} and \mathcal{E} .

the six blocks (\mathcal{L} , \mathcal{G} , W , $\bar{\Lambda}$, \mathcal{E} , \mathcal{N}) for solving (29) yields the iteration scheme alternatingly as follows:

$$\begin{cases} W^+ = \min_W H_1(W) + H_2(W) + \frac{\rho^*}{2} \|W - W^*\|_F^2, \\ \mathcal{G}^+ = \min_{\mathcal{G}} H_1(\mathcal{G}) + \langle \mathcal{G} - \mathcal{G}^*, \nabla H_5(\mathcal{G}^*) \rangle \\ + \frac{\rho^*}{2} \|\mathcal{G} - \mathcal{G}^*\|_F^2, \\ \bar{\Lambda}^+ = \min_{\bar{\Lambda}} H_2(\bar{\Lambda}) + \frac{\rho^*}{2} \|\bar{\Lambda} - \bar{\Lambda}^*\|_F^2, \\ \mathcal{L}^+ = \min_{\mathcal{L}} H_5(\mathcal{L}) + H_6(\mathcal{L}) + \frac{\rho^*}{2} \|\mathcal{L} - \mathcal{L}^*\|_F^2, \\ \mathcal{E}^+ = \min_{\mathcal{E}} H_3(\mathcal{E}) + H_6(\mathcal{E}) + \frac{\rho^*}{2} \|\mathcal{E} - \mathcal{E}^*\|_F^2, \\ \mathcal{N}^+ = \min_{\mathcal{N}} H_4(\mathcal{N}) + H_6(\mathcal{N}) + \frac{\rho^*}{2} \|\mathcal{N} - \mathcal{N}^*\|_F^2, \end{cases} \quad (41)$$

Based on Theorem 8, W and \mathcal{G} are updated as follows:

$$W_{j,i}^+ = \max \left(\frac{\gamma \bar{\Lambda}_{j,i}^* + \rho W_{j,i}^* - \log \left(\frac{\sigma_j(\mathcal{G}^{*(i)})}{\epsilon} + 1 \right)}{\gamma + \rho^*}, 0 \right), \quad (42)$$

$$\mathcal{G}^+ = \mathcal{U} * \mathcal{S}_1 * \mathcal{V}^H, \quad (43)$$

where \mathcal{U} and \mathcal{V} are derived from the t-SVD of $\mathcal{G}^* + \frac{\mu \mathcal{L}^* + \mathcal{R}^* - \mu \mathcal{G}^*}{\rho^*} = \mathcal{U} * \mathcal{S}_2 * \mathcal{V}^H$. The relationship between \mathcal{S}_1 and \mathcal{S}_2 is given by Theorem 8.

The update for $\bar{\Lambda}$ turns out to be straightforward:

$$\bar{\Lambda}^+ = \frac{\gamma W^+ + \rho^* \bar{\Lambda}^*}{\gamma + \rho^*}. \quad (44)$$

Fixed $\mathcal{G}_{k_1 k_2}$, \mathcal{E} , \mathcal{N} , $\mathcal{R}_{k_1 k_2}$ and \mathcal{F} , the minimization problem \mathcal{L} is converted into the following form:

$$\begin{aligned} \min_{\mathcal{L}} \sum_{1 \leq l_1 < l_2 \leq N} \beta_{k_1 k_2} \frac{\mu_{k_1 k_2}}{2} \|\mathcal{L} - \mathcal{G}_{k_1 k_2}^+\|_F^2 + \frac{\mathcal{R}_{k_1 k_2}^*}{\mu_{k_1 k_2}} \|\mathcal{F}\|_F^2 \\ + \frac{\tau}{2} \|\mathcal{T} - \mathcal{L} - \mathcal{E}^* - \mathcal{N}^* + \frac{\mathcal{F}}{\tau}\|_F^2 + \frac{\rho^*}{2} \|\mathcal{L} - \mathcal{L}^*\|_F^2. \end{aligned} \quad (45)$$

The closed form of \mathcal{L} can be derived by setting the derivative of (45) to zero. We can now update \mathcal{L} by the following equation:

$$\mathcal{L}^+ = \frac{\mathcal{S}}{\sum \mu_{k_1 k_2} + \tau + \rho^*}, \quad (46)$$

where $\mathcal{S} = \sum \mu_{k_1 k_2} \mathcal{G}_{k_1 k_2}^+ - \mathcal{R}_{k_1 k_2}^* + \tau(\mathcal{T} - \mathcal{E}^* - \mathcal{N}^*) + \mathcal{F}^* + \rho^* \mathcal{L}^*$.

Now, let's solve \mathcal{E} . The minimization problem of \mathcal{E} is as follows:

$$\begin{aligned} & \min_{\mathcal{E}} \tau_1 \|\mathcal{E}\|_1 + \frac{\rho^*}{2} \|\mathcal{E} - \mathcal{E}^*\|_F^2 \\ & + \frac{\tau}{2} \|\mathcal{T} - \mathcal{L}^+ - \mathcal{E} - \mathcal{N}^* + \frac{\mathcal{F}^*}{\tau}\|_F^2. \end{aligned} \quad (47)$$

Problem (47) has the following closed-form solution:

$$\mathcal{E}^+ = S_{\frac{\tau_1}{\tau + \rho^*}} \left(\frac{\tau(\mathcal{T} - \mathcal{L}^+ + \frac{\mathcal{F}^*}{\tau}) + \rho^* \mathcal{E}^*}{\tau + \rho^*} \right), \quad (48)$$

where $S_\lambda(\cdot)$ is the soft thresholding operator [44]:

$$S_\lambda(x) = \begin{cases} 0, & \text{if } |x| \leq \lambda, \\ \text{sign}(x)(|x| - \lambda), & \text{if } |x| > \lambda \end{cases} \quad (49)$$

The minimization problem of \mathcal{N} is as follows:

$$\min_{\mathcal{N}} \tau_2 \|\mathcal{N}\|_F^2 + \frac{\tau}{2} \|\mathcal{T} - \mathcal{L}^+ - \mathcal{E}^+ - \mathcal{N} + \frac{\mathcal{F}^*}{\tau}\|_F^2 + \frac{\rho^*}{2} \|\mathcal{N} - \mathcal{N}^*\|_F^2.$$

We update \mathcal{N} by the following equation:

$$\mathcal{N}^+ = \frac{\tau(\mathcal{T} - \mathcal{L}^+ - \mathcal{E}^+) + \mathcal{F}^* + \rho^* \mathcal{N}^*}{2\tau_2 + \tau + \rho^*}. \quad (50)$$

Finally, multipliers $\mathcal{R}_{k_1 k_2}$ and \mathcal{F} are updated according to the following formula:

$$\begin{cases} \mathcal{R}_{k_1 k_2}^+ = \mathcal{R}_{k_1 k_2}^* + \mu_{k_1 k_2} (\mathcal{L}^+ - \mathcal{G}_{k_1 k_2}^+); \\ \mathcal{F}^+ = \mathcal{F}^* + \tau(\mathcal{T} - \mathcal{L}^+ - \mathcal{E}^+ - \mathcal{N}^+). \end{cases} \quad (51)$$

EMLCP-based TPRCA model computation is given in Algorithm 2. The main per-iteration cost lies in the update of $\mathcal{G}_{k_1 k_2}$, which requires computing SVD and t-SVD. The per-iteration complexity is $O(LE(\sum_{1 \leq k_1 < k_2 \leq N} [\log(\text{le}_{k_1 k_2}) + \min(I_{k_1}, I_{k_2})]))$, where $LE = \prod_{i=1}^N I_i$ and $\text{le}_{k_1 k_2} = LE / (I_{k_1} I_{k_2})$.

V. CONVERGENCE ANALYSIS

In this section, the convergence of PALM is established under some mild conditions, which is mainly based on the framework in [40].

Theorem 9: Suppose that $\rho_1 = \gamma_1 \mu$ with $\gamma_1 > 1$. Let the sequence $\{(\mathcal{Z}, \mathcal{M}, W, \bar{\Lambda})\}$ be generated by Algorithm 1. Then,

- (a) any accumulation point of the sequence $\{(\mathcal{Z}^k, \mathcal{M}^k, W^k, \bar{\Lambda}^k)\}$ is a critical point of (27).
- (b) if H_1 is KL functions, the sequence $\{(\mathcal{Z}^k, \mathcal{M}^k, W^k, \bar{\Lambda}^k)\}$ converges to a critical point of (27).

Proof: First, in the solution process, only the non-convex function $H_1(\mathcal{M})$ is included in the iteration of \mathcal{M} , and the updates of other elements are solved by convex functions. The variables solved by the convex function are strictly descending, hence we get the following inequality:

$$\begin{aligned} & H_1(W^{k+1}) + H_2(W^{k+1}) + \frac{\rho^k}{2} \|W^{k+1} - W^k\|_F^2 \\ & \leq H_1(W^k) + H_2(W^k) + \frac{\rho^k}{2} \|W^k - W^k\|_F^2, \end{aligned} \quad (52)$$

$$H_2(\bar{\Lambda}^{k+1}) + \frac{\rho^k}{2} \|\bar{\Lambda}^{k+1} - \bar{\Lambda}^k\|_F^2 \leq H_2(\bar{\Lambda}^k), \quad (53)$$

$$H_3(\mathcal{Z}^{k+1}) + \frac{\rho^k}{2} \|\mathcal{Z}^{k+1} - \mathcal{Z}^k\|_F^2 \leq H_3(\mathcal{Z}^k), \quad (54)$$

By the definition of $H_3(\mathcal{M}, \mathcal{Z})$ in (30), the gradients of H_3 with respect to \mathcal{M} and \mathcal{Z} , respectively, are

$$\nabla_{\mathcal{M}} H_3(\mathcal{M}, \mathcal{Z}) = \mu(\mathcal{M} - \mathcal{Z} - \frac{\mathcal{Q}}{\mu}), \quad (55)$$

$$\nabla_{\mathcal{Z}} H_3(\mathcal{M}, \mathcal{Z}) = \mu(\mathcal{Z} - \mathcal{M} + \frac{\mathcal{Q}}{\mu}). \quad (56)$$

For any fixed \mathcal{Z} , we obtain that

$$\begin{aligned} & \|\nabla_{\mathcal{M}} H_3(\mathcal{M}_1, \mathcal{Z}) - \nabla_{\mathcal{M}} H_3(\mathcal{M}_2, \mathcal{Z})\|_F \\ & = \|\mu(\mathcal{M}_1 - \mathcal{Z} - \frac{\mathcal{Q}}{\mu}) - \mu(\mathcal{M}_2 - \mathcal{Z} - \frac{\mathcal{Q}}{\mu})\|_F \\ & = \mu \|\mathcal{M}_1 - \mathcal{M}_2\|_F, \end{aligned} \quad (57)$$

and for any fixed \mathcal{M} , we get that

$$\begin{aligned} & \|\nabla_{\mathcal{Z}} H_3(\mathcal{M}, \mathcal{Z}_1) - \nabla_{\mathcal{Z}} H_3(\mathcal{M}, \mathcal{Z}_2)\|_F \\ & = \|\mu(\mathcal{Z}_1 - \mathcal{M} + \frac{\mathcal{Q}}{\mu}) - \mu(\mathcal{Z}_2 - \mathcal{M} + \frac{\mathcal{Q}}{\mu})\|_F \\ & = \mu \|\mathcal{Z}_1 - \mathcal{Z}_2\|_F. \end{aligned} \quad (58)$$

(57) and (58) imply that the gradient of $H_3(\mathcal{M}, \mathcal{Z})$ is Lipschitz continuous block-wise. Note that $H_3(\mathcal{M}, \mathcal{Z})$ is twice continuously differentiable, which brings that $\nabla H_3(\mathcal{M}, \mathcal{Z})$ is Lipschitz continuous on bounded subsets of $\mathbb{R}^{I_1 \times I_2 \times \dots \times I_N} \times \mathbb{R}^{I_1 \times I_2 \times \dots \times I_N}$ [40]. So

$$\begin{aligned} & H_3(\mathcal{M}^{k+1}) + H_1(\mathcal{M}^{k+1}) + \frac{(\gamma_1 - 1)\mu}{2} \|\mathcal{M}^{k+1} - \mathcal{M}^k\|_F^2 \\ & \leq H_3(\mathcal{M}^k) + H_1(\mathcal{M}^k). \end{aligned} \quad (59)$$

From [40], we get that

$$\begin{aligned} & LAG(\mathcal{Z}^{k+1}, \mathcal{M}^{k+1}, W^{k+1}, \bar{\Lambda}^{k+1}) \\ & + \frac{(\gamma_1 - 1)\mu}{2} \|\mathcal{M}^{k+1} - \mathcal{M}^k\|_F^2 + \frac{\rho^k}{2} (\|W^{k+1} - W^k\|_F^2) \\ & + \frac{\rho^k}{2} (\|\bar{\Lambda}^{k+1} - \bar{\Lambda}^k\|_F^2 + \|\mathcal{Z}^{k+1} - \mathcal{Z}^k\|_F^2) \\ & \leq LAG(\mathcal{Z}^k, \mathcal{M}^k, W^k, \bar{\Lambda}^k), \end{aligned} \quad (60)$$

and

$$\begin{aligned} & \lim_{k \rightarrow +\infty} \|\mathcal{M}^{k+1} - \mathcal{M}^k\|_F \\ & = \lim_{k \rightarrow +\infty} \|W^{k+1} - W^k\|_F \\ & = \lim_{k \rightarrow +\infty} \|\bar{\Lambda}^{k+1} - \bar{\Lambda}^k\|_F \\ & = \lim_{k \rightarrow +\infty} \|\mathcal{Z}^{k+1} - \mathcal{Z}^k\|_F = 0. \end{aligned} \quad (61)$$

(a) Assume that there exists a subsequence $\{(\mathcal{Z}^{k_j}, \mathcal{M}^{k_j}, W^{k_j}, \bar{\Lambda}^{k_j})\}$ of $\{(\mathcal{Z}^k, \mathcal{M}^k, W^k, \bar{\Lambda}^k)\}$ such that $\{(\mathcal{Z}^{k_j}, \mathcal{M}^{k_j}, W^{k_j}, \bar{\Lambda}^{k_j})\}$ converges to $(\mathcal{Z}^*, \mathcal{M}^*, W^*, \bar{\Lambda}^*)$ as $j \rightarrow +\infty$. By (61), we have that $\{(\mathcal{Z}^{k_j}, \mathcal{M}^{k_j}, W^{k_j}, \bar{\Lambda}^{k_j})\}$ also converges to $(\mathcal{Z}^*, \mathcal{M}^*, W^*, \bar{\Lambda}^*)$ as $j \rightarrow +\infty$. Moreover, the optimality conditions of (31) gives that

$$0 = \nabla H_1(W^{k_j+1}) + \nabla H_2(W^{k_j+1}) + \rho^k (W^{k_j+1} - W^{k_j}),$$

$$0 \in \partial H_1(\mathcal{M}^{k_j+1}) - \mu(\mathcal{Z} - \mathcal{M}^{k_j} + \frac{\mathcal{Q}}{\mu}) + \rho_1^k (\mathcal{M}^{k_j+1} - \mathcal{M}^{k_j}),$$

$$0 = \nabla H_2(\bar{\Lambda}^{k_{j+1}}) + \rho^k(\bar{\Lambda}^{k_{j+1}} - \bar{\Lambda}^{k_j}),$$

$$0 = \nabla H_3(\mathcal{Z}^{k_{j+1}}) + \rho^k(\mathcal{Z}^{k_{j+1}} - \mathcal{Z}^{k_j}),$$

When $j \rightarrow +\infty$, by [45], we get that

$$0 = \nabla H_1(W^*) + \nabla H_2(W^*),$$

$$0 \in \partial H_1(\mathcal{M}^*) - \mu(\mathcal{Z} - \mathcal{M}^* + \frac{Q}{\mu}) = \partial H_1(\mathcal{M}^*) + \nabla H_3(\mathcal{M}^*),$$

$$0 = \nabla H_2(\bar{\Lambda}^*),$$

$$0 = \nabla H_3(\mathcal{Z}^*),$$

Therefore, we obtain that

$$(0, 0, 0, 0) \in \partial LAG(\mathcal{Z}^*, \mathcal{M}^*, W^*, \bar{\Lambda}^*) \quad (62)$$

which implies that $(\mathcal{Z}^*, \mathcal{M}^*, W^*, \bar{\Lambda}^*)$ is a critical point of $LAG(\mathcal{Z}, \mathcal{M}, W, \bar{\Lambda})$.

(b) By the definition of $LAG(\mathcal{Z}, \mathcal{M}, W, \bar{\Lambda})$, we have that $LAG(\mathcal{Z}, \mathcal{M}, W, \bar{\Lambda}) \rightarrow +\infty$ as $\|(\mathcal{Z}, \mathcal{M}, W, \bar{\Lambda})\|_F \rightarrow +\infty$. Suppose that $(\mathcal{Z}^k, \mathcal{M}^k, W^k, \bar{\Lambda}^k)$ is unbounded, i.e., $\|(\mathcal{Z}^k, \mathcal{M}^k, W^k, \bar{\Lambda}^k)\|_F \rightarrow +\infty$, we derive that $LAG(\mathcal{Z}^k, \mathcal{M}^k, W^k, \bar{\Lambda}^k) \rightarrow +\infty$. However, it follows from (60) that $LAG(\mathcal{Z}^k, \mathcal{M}^k, W^k, \bar{\Lambda}^k)$ is upper bounded. Therefore, the sequence $\{(\mathcal{Z}^k, \mathcal{M}^k, W^k, \bar{\Lambda}^k)\}$ is bounded. From [39], Logarithmic function is KL function. Thus, H_1 also KL function. Notice that H_2 and H_3 are KL function, we have that $LAG(\mathcal{Z}^k, \mathcal{M}^k, W^k, \bar{\Lambda}^k)$ is also a KL function [40]. Then by [40], we obtain that the sequence $\{(\mathcal{Z}^k, \mathcal{M}^k, W^k, \bar{\Lambda}^k)\}$ converges to a critical point of (27). ■

Theorem 10: Suppose that $\rho_1 = \gamma_1 \mu$ with $\gamma_1 > 1$. Let the sequence $\{(\mathcal{L}, \mathcal{G}, W, \bar{\Lambda}, \mathcal{E}, \mathcal{N})\}$ be generated by Algorithm 2. Then,

(a) any accumulation point of the sequence $\{(\mathcal{L}, \mathcal{G}, W, \bar{\Lambda}, \mathcal{E}, \mathcal{N})\}$ is a critical point of (38).

(b) if H_1 is KL functions and coercive, the sequence $\{(\mathcal{L}, \mathcal{G}, W, \bar{\Lambda}, \mathcal{E}, \mathcal{N})\}$ converges to a critical point of (38).

Proof: Compared with LRTC, the TRPCA algorithm has two more variables, \mathcal{E} and \mathcal{N} , but its solutions are all convex functions. Therefore, the convergence proof of the TRPCA algorithm is similar to that of the LRTC algorithm, and will not be repeated here. ■

VI. EXPERIMENTS

We evaluate the performance of the proposed EMLCP-based LRTC and TRPCA methods. All methods are tested on real-world data. We employ the peak signal-to-noise rate (PSNR) value, the structural similarity (SSIM) value [46], the feature similarity (FSIM) value [47], and erreur relative globale adimensionnelle de synthèse (ERGAS) value [48] to measure the quality of the recovered results. The PSNR, SSIM and FSIM value are the bigger the better, and the ERGAS value is the smaller the better. For simplicity, EMLCP-based LRTC and EMLCP-based TRPCA are denoted as EMLCP. All tests are implemented on the Windows 10 platform and MATLAB (R2019a) with an Intel Core i7-10875H 2.30 GHz and 32 GB of RAM.

A. Low-rank tensor completion

In this section, we test three kinds of real-world data: MSI, MRI and CV. The method for sampling the data is purely random sampling. The comparative LRTC methods are as follows: HaLRTC [49], and LRTCTV-I [50] represent state-of-the-art for the Tucker-decomposition-based methods; TNN [27], PSTNN [51], FTNN [52], WSTNN [28], and nonconvex WSTNN [53] represent state-of-the-art for the t-SVD-based methods; and minmax concave plus penalty-based TC method (McpTC) [54]. Since the TNN, PSTNN, and FTNN methods are only applicable to three-order tensors, in all four-order tensor tests, we first reshape the four-order tensor into three-order tensors and then test the performances of these methods. It is not difficult to find that the NWSTNN method in the comparison method adopts the non-convex relaxation of the Logarithmic function, and the results obtained by comparing with such method are consistent with our theory property.

1) *MSI completion:* We test 32 MSIs in the dataset CAVE¹. All testing data are of size $256 \times 256 \times 31$. In Fig.1, we randomly select three from 32 MSIs, and brings the different sampling rate and different band visual results. The individual MSI names and their corresponding bands are written in the caption of Fig.1. As can be seen from Fig.1, the visual effect of the EMLCP method is superior to the NWSTNN method under all sample rate, which is consistent with our theory. To further highlight the superiority of our method, the average quantitative results of 32 MSIs are listed in Table I. The results show that the PSNR value of our algorithms is 0.4dB higher than that of the suboptimal method when the sampling rate is 20%, and even reaches 0.8dB when the sampling rate is 5%. More experimental results are available in the Appendix K.

2) *MRI completion:* We test the performance of the proposed method and the comparative method on MRI² data with the size of $181 \times 217 \times 181$. First, we demonstrate the visual effect recovered by MRI data at sampling rates of 5%, 10% and 20% in Fig.2. Our method is clearly superior to the comparative methods. Then, we list the average quantitative results of frontal slices of MRI restored by all methods at different sampling rates in Table II. Obviously, the PSNR value of our method is at average 0.3dB higher than that of the suboptimal method, and the values of SSIM, FSIM and ERGAS are significantly better than that of the suboptimal method.

3) *CV completion:* We test nine CVs³(respectively named news, akiyo, hall, highway, foreman, container, coastguard, suzie, carphone) of size $144 \times 176 \times 3 \times 50$. Firstly, we list the average quantitative results of 9 CVs in Table III. At this time, the suboptimal method is the NWSTNN method. The PSNR value of our method is average 0.4dB higher than it at three sampling rates. Furthermore, we demonstrate the visual results of 9 CVs in our experiment in Fig.3, in which the number of frames and sampling rate corresponding to each CV are described in the caption of Fig.3. It is not hard to see from the picture that the recovery of our method on the vision

¹<http://www.cs.columbia.edu/CAVE/databases/multispectral/>

²http://brainweb.bic.mni.mcgill.ca/brainweb/selection_normal.html

³<http://trace.eas.asu.edu/yuv/>

TABLE I
THE AVERAGE PSNR, SSIM, FSIM AND ERGAS VALUES FOR 32 MSIS TESTED BY OBSERVED AND THE NINE UTILIZED LRTC METHODS.

SR	5%				10%				20%			
	Method	PSNR	SSIM	FSIM	ERGAS	PSNR	SSIM	FSIM	ERGAS	PSNR	SSIM	FSIM
Observed	15.438	0.153	0.644	845.388	15.673	0.194	0.646	822.788	16.184	0.269	0.650	775.866
HaLRTC	18.112	0.285	0.697	689.482	22.694	0.527	0.786	478.325	32.175	0.835	0.910	190.848
TNN	17.986	0.247	0.685	726.893	28.627	0.678	0.861	314.352	40.170	0.964	0.972	59.018
LRTCTV-I	25.894	0.800	0.835	276.620	30.709	0.890	0.906	162.567	35.486	0.949	0.957	94.646
McpTC	32.459	0.875	0.909	133.472	35.959	0.925	0.943	91.788	40.518	0.964	0.972	56.083
PSTNN	18.713	0.474	0.650	574.637	23.239	0.683	0.783	352.012	34.206	0.924	0.942	117.472
FTNN	32.620	0.899	0.924	131.871	37.182	0.954	0.963	78.694	43.002	0.984	0.987	41.625
WSTNN	31.439	0.806	0.911	208.988	40.170	0.981	0.981	52.895	47.059	0.995	0.995	24.914
NWSTNN	37.417	0.945	0.950	71.261	43.704	0.985	0.985	35.779	51.362	0.997	0.997	15.572
EMLCP	38.298	0.962	0.964	64.689	44.340	0.988	0.988	33.329	51.742	0.997	0.997	14.779

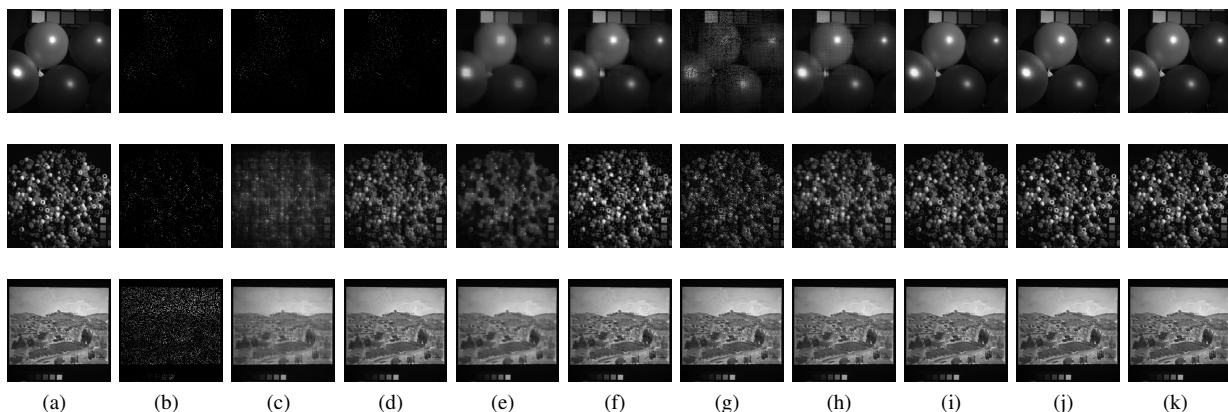


Fig. 1. (a) Original image. (b) Observed image. (c) HaLRTC. (d) TNN. (e) LRTCTV-I. (f) McpTC. (g) PSTNN. (h) FTNN. (i) WSTNN. (j) NWSTNN. (k) EMLCP. SR: top row is 5%, middle row is 10% and last row is 20%. The rows of MSIs are in order: balloons, beads, watercolors. The corresponding bands in each row are: 31, 20, 10.

TABLE II
THE PSNR, SSIM, FSIM AND ERGAS VALUES OUTPUT BY OBSERVED AND THE NINE UTILIZED LRTC METHODS FOR MRI.

SR	5%				10%				20%			
	Method	PSNR	SSIM	FSIM	ERGAS	PSNR	SSIM	FSIM	ERGAS	PSNR	SSIM	FSIM
Observed	11.399	0.310	0.530	1021.071	11.633	0.323	0.565	994.049	12.149	0.350	0.613	936.747
HaLRTC	17.372	0.301	0.638	532.927	20.105	0.439	0.726	391.945	24.451	0.659	0.829	235.019
TNN	22.681	0.470	0.742	303.284	26.064	0.643	0.812	205.410	29.972	0.798	0.882	130.791
LRTCTV-I	19.400	0.598	0.702	431.241	22.864	0.749	0.805	294.937	28.236	0.891	0.908	155.272
McpTC	27.931	0.748	0.843	154.029	31.439	0.844	0.888	102.744	35.576	0.937	0.941	63.906
PSTNN	17.064	0.243	0.639	542.819	22.870	0.487	0.757	297.337	29.083	0.772	0.870	145.165
FTNN	24.673	0.687	0.836	234.329	28.297	0.820	0.896	152.733	32.767	0.919	0.947	89.543
WSTNN	25.524	0.708	0.825	211.315	29.059	0.837	0.888	139.177	33.497	0.928	0.940	82.851
NWSTNN	30.222	0.826	0.884	119.820	33.293	0.902	0.924	83.608	36.860	0.950	0.956	54.962
EMLCP	30.563	0.850	0.893	115.395	33.643	0.918	0.932	80.590	37.180	0.959	0.962	53.344

effect is better. More experimental results are available in the Appendix L.

B. Tensor robust principal component analysis

In this section, we evaluate the performance of the proposed TRPCA method through HSI mixed noise denoising. The comparative TRPCA methods include the SNN [55], TNN [41], 3DTNN and 3DLogTNN [53] methods.

1) *HSI denoising*: We test the Pavia University data sets and Washington DC Mall data sets, where Pavia University data size is $200 \times 200 \times 80$ and Washington DC Mall data size

is $256 \times 256 \times 150$. We divide the mixed noise into two kinds, one is independent identically distributed Gaussian noise plus independent identically distributed pepper and salt noise, and the other is non i.i.d. Gaussian noise plus i.i.d pepper and salt noise, where σ is pepper and salt noise and ν is Gaussian noise. In Table IV, we list the quantitative numerical results of Pavia University and Washington DC Mall Data under 3 combinations of these two kinds of noise respectively. It can be seen that under the influence of the weakest noise, the PSNR value of the obtained results is 0.6 dB higher than that of the suboptimal method 3DLogTNN. Even under the influence

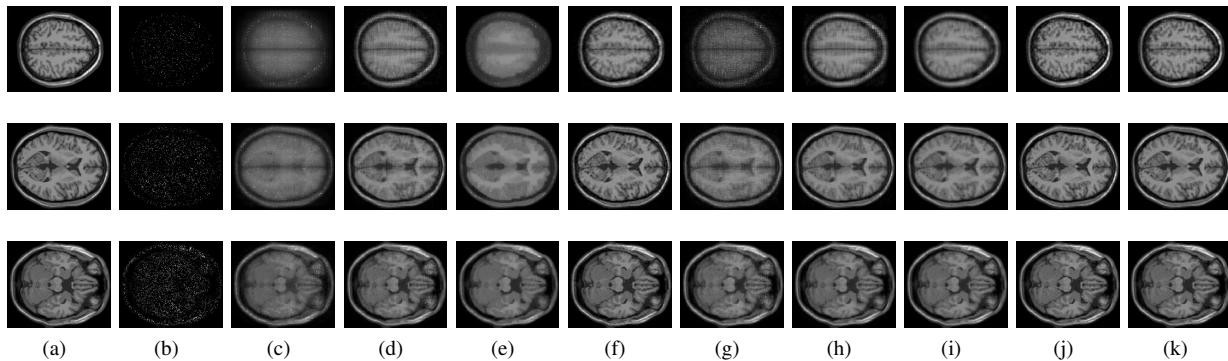


Fig. 2. (a) Original image. (b) Observed image. (c) HaLRTC. (d) TNN. (e) LRTCTV-I. (f) McpTC. (g) PSTNN. (h) FTNN. (i) WSTNN. (j) NWSTNN. (k) EMLCP. Each type of slice: the first row is the 120th slice with a sampling rate of 5%, the second row is the 80th slice with a sampling rate of 10%, and the third row is the 50th slice with a sampling rate of 20%.

TABLE III
THE AVERAGE PSNR, SSIM, FSIM AND ERGAS VALUES FOR 9 CVs TESTED BY OBSERVED AND THE NINE UTILIZED LRTC METHODS.

SR	5%				10%				20%			
	PSNR	SSIM	FSIM	ERGAS	PSNR	SSIM	FSIM	ERGAS	PSNR	SSIM	FSIM	ERGAS
Observed	6.129	0.012	0.431	1170.276	6.363	0.019	0.428	1139.091	6.875	0.033	0.426	1073.940
HaLRTC	17.439	0.497	0.700	329.176	21.207	0.625	0.776	214.604	25.178	0.775	0.864	135.612
TNN	26.940	0.764	0.881	114.770	30.092	0.845	0.922	82.293	33.193	0.902	0.950	59.164
LRTCTV-I	19.945	0.598	0.708	259.639	21.864	0.674	0.786	213.126	26.458	0.826	0.888	119.600
McpTC	23.799	0.669	0.822	161.726	28.480	0.817	0.898	93.541	31.195	0.885	0.934	68.258
PSTNN	15.274	0.307	0.670	409.255	26.822	0.776	0.886	114.335	32.739	0.900	0.948	61.799
FTNN	25.563	0.768	0.872	133.678	28.718	0.856	0.917	92.039	32.209	0.922	0.952	61.699
WSTNN	29.128	0.869	0.916	89.451	32.341	0.919	0.948	63.735	36.049	0.957	0.972	42.622
NWSTNN	30.230	0.845	0.927	81.396	34.002	0.911	0.956	54.680	38.520	0.960	0.980	32.930
EMLCP	30.872	0.871	0.934	75.578	34.570	0.926	0.961	51.204	38.752	0.966	0.981	31.756



Fig. 3. (a) Original image. (b) Observed image. (c) HaLRTC. (d) TNN. (e) LRTCTV-I. (f) McpTC. (g) PSTNN. (h) FTNN. (i) WSTNN. (j) NWSTNN. (k) EMLCP. SR: top row is 5%, middle row is 10% and last row is 20%. The rows of CVs are in order: the 15th frame of news, the 30th frame of foreman, the 45th frame of suzie.

of the most severe noise, the PSNR value of the obtained results is still better than the suboptimal method 3DLogTNN. In Fig.4, we show the visual results of the two kinds of data in turn according to the order of noise levels in Table IV. The corresponding spectral bands are 50, 30, 100 respectively. It is easy to find from the figure that our method has better denoising effect than the comparative method.

VII. CONCLUSION

In this paper, we propose MLCP function, a new non-convex function, which finds that the Logarithmic function is the

upper bound of the MLCP function. It is theoretically guaranteed that the MLCP function can achieve better results for the minimization problem. The proposed function is directly applied to the tensor recovery problem, its explicit solution cannot be obtained, which is very unfavorable to the solution of the algorithm. To this end, we further put forward the corresponding equivalence theorem to settle this problem. We apply the equivalent weighted tensor $L\gamma$ -norm to the LRTC and TRPCA problems, giving their EMLCP-based models respectively. According to the Kurdyka-Łojasiewicz property, we prove that the solution sequence of the proposed algorithm has finite length and converges globally to a critical point.

TABLE IV
THE PSNR, SSIM AND FSIM VALUES FOR 2 HSI TESTED BY OBSERVED AND THE NINE UTILIZED LRTC METHODS.

HSI	Mixed noise		Noise	SNN	TNN	3DTNN	3DLogTNN	EMLCP
Pavia City Center	$\sigma = 0.05 \nu = 0.2$	PSNR	11.646	26.899	27.920	35.833	37.231	37.825
		SSIM	0.119	0.788	0.780	0.969	0.974	0.976
		FSIM	0.532	0.868	0.890	0.979	0.982	0.984
	$\sigma = 0.1 \nu = 0.2$	PSNR	11.198	24.290	22.647	31.946	33.647	33.890
		SSIM	0.105	0.632	0.527	0.928	0.943	0.945
		FSIM	0.493	0.789	0.778	0.952	0.962	0.963
	σ follows U(0.1-0.15) $\nu = 0.2$	PSNR	10.846	23.441	20.905	30.623	32.469	32.528
		SSIM	0.095	0.566	0.432	0.903	0.927	0.927
		FSIM	0.473	0.757	0.732	0.937	0.951	0.952
Washington DC	$\sigma = 0.05 \nu = 0.2$	PSNR	11.279	27.737	28.002	36.428	38.767	39.448
		SSIM	0.116	0.794	0.750	0.959	0.979	0.980
		FSIM	0.517	0.883	0.882	0.978	0.986	0.988
	$\sigma = 0.1 \nu = 0.2$	PSNR	10.866	25.328	22.875	31.391	35.017	35.332
		SSIM	0.103	0.671	0.510	0.872	0.950	0.951
		FSIM	0.476	0.822	0.768	0.937	0.969	0.971
	σ follows U(0.1-0.15) $\nu = 0.2$	PSNR	10.549	24.528	21.165	29.175	33.621	33.790
		SSIM	0.094	0.623	0.424	0.798	0.935	0.935
		FSIM	0.457	0.796	0.723	0.905	0.961	0.963

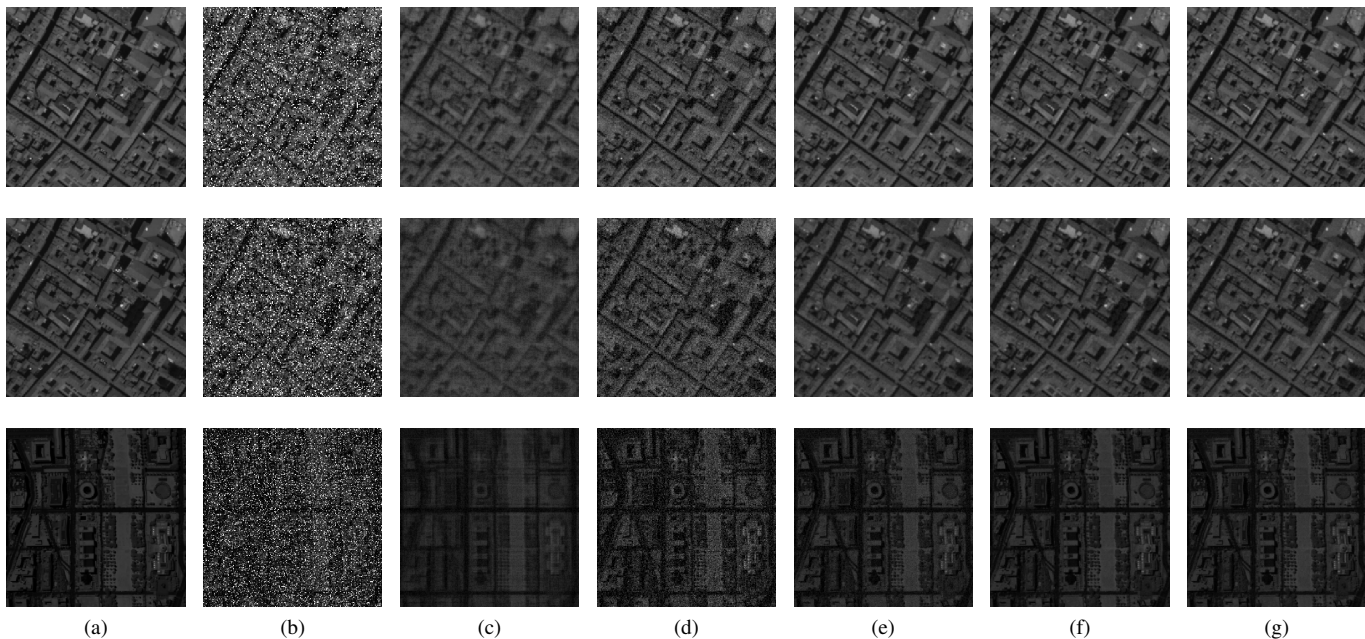


Fig. 4. (a) Original image. (b) Noise image. (c) SNN. (d) TNN. (e) 3DTNN. (f) 3DLogTNN. (g) EMLCP

Extensive experiments show that our method can achieve good visual and numerical quantitative results. The obtained numerical quantitative results outperform the NWSTNN method using Logarithmic function, which is consistent with our theoretical analysis. In addition, it is worth studying whether the MLCP function can be extended in more applications.

REFERENCES

- [1] Y.-M. Huang, H.-Y. Yan, Y.-W. Wen, and X. Yang, "Rank minimization with applications to image noise removal," *Information Sciences*, vol. 429, pp. 147–163, 2018.
- [2] B. Madathil and S. N. George, "Twist tensor total variation regularized-reweighted nuclear norm based tensor completion for video missing area recovery," *Information Sciences*, vol. 423, pp. 376–397, 2018.
- [3] Y. Wang, D. Meng, and M. Yuan, "Sparse recovery: from vectors to tensors," *National Science Review*, vol. 5, no. 5, pp. 756–767, 2018.
- [4] X.-L. Zhao, W.-H. Xu, T.-X. Jiang, Y. Wang, and M. K. Ng, "Deep plug-and-play prior for low-rank tensor completion," *Neurocomputing*, vol. 400, pp. 137–149, 2020.
- [5] S. Li, R. Dian, L. Fang, and J. M. Bioucas-Dias, "Fusing hyperspectral and multispectral images via coupled sparse tensor factorization," *IEEE Transactions on Image Processing*, vol. 27, no. 8, pp. 4118–4130, 2018.
- [6] X. Fu, W.-K. Ma, J. M. Bioucas-Dias, and T.-H. Chan, "Semiblind hyperspectral unmixing in the presence of spectral library mismatches," *IEEE Transactions on Geoscience and Remote Sensing*, vol. 54, no. 9, pp. 5171–5184, 2016.
- [7] J. Xue, Y. Zhao, W. Liao, and J. C.-W. Chan, "Nonlocal low-rank regularized tensor decomposition for hyperspectral image denoising," *IEEE Transactions on Geoscience and Remote Sensing*, vol. 57, no. 7, pp. 5174–5189, 2019.
- [8] J. Xue, Y. Zhao, W. Liao, J. C.-W. Chan, and S. G. Kong, "Enhanced sparsity prior model for low-rank tensor completion," *IEEE Transactions on Neural Networks and Learning Systems*, vol. 31, no. 11, pp. 4567–4581, 2020.

- [9] H. Zhang, X. Liu, H. Fan, Y. Li, and Y. Ye, "Fast and accurate low-rank tensor completion methods based on qr decomposition and $l_{\{2, 1\}}$ norm minimization," *arXiv preprint arXiv:2108.03002*, 2021.
- [10] J.-H. Yang, X.-L. Zhao, T.-Y. Ji, T.-H. Ma, and T.-Z. Huang, "Low-rank tensor train for tensor robust principal component analysis," *Applied Mathematics and Computation*, vol. 367, p. 124783, 2020.
- [11] T.-X. Jiang, T.-Z. Huang, X.-L. Zhao, T.-Y. Ji, and L.-J. Deng, "Matrix factorization for low-rank tensor completion using framelet prior," *Information Sciences*, vol. 436, pp. 403–417, 2018.
- [12] M. Ding, T.-Z. Huang, T.-Y. Ji, X.-L. Zhao, and J.-H. Yang, "Low-rank tensor completion using matrix factorization based on tensor train rank and total variation," *Journal of Scientific Computing*, vol. 81, no. 2, pp. 941–964, 2019.
- [13] J. Xue, Y. Zhao, W. Liao, and J. Cheung-Wai Chan, "Nonconvex tensor rank minimization and its applications to tensor recovery," *Information Sciences*, vol. 503, pp. 109–128, 2019.
- [14] J. Xue, Y. Zhao, W. Liao, and J. Cheung-Wai Chan, "Total variation and rank-1 constraint rpca for background subtraction," *IEEE Access*, vol. 6, pp. 49 955–49 966, 2018.
- [15] I. Kajo, N. Kamel, Y. Ruichek, and A. S. Malik, "Svd-based tensor-completion technique for background initialization," *IEEE Transactions on Image Processing*, vol. 27, no. 6, pp. 3114–3126, 2018.
- [16] W. Cao, Y. Wang, J. Sun, D. Meng, C. Yang, A. Cichocki, and Z. Xu, "Total variation regularized tensor rpca for background subtraction from compressive measurements," *IEEE Transactions on Image Processing*, vol. 25, no. 9, pp. 4075–4090, 2016.
- [17] W. Wei, L. Yi, Q. Xie, Q. Zhao, D. Meng, and Z. Xu, "Should we encode rain streaks in video as deterministic or stochastic?" in *2017 IEEE International Conference on Computer Vision (ICCV)*, 2017, pp. 2535–2544.
- [18] M. Li, Q. Xie, Q. Zhao, W. Wei, S. Gu, J. Tao, and D. Meng, "Video rain streak removal by multiscale convolutional sparse coding," in *2018 IEEE/CVF Conference on Computer Vision and Pattern Recognition*, 2018, pp. 6644–6653.
- [19] Q. Zhao, L. Zhang, and A. Cichocki, "Bayesian cp factorization of incomplete tensors with automatic rank determination," *IEEE Transactions on Pattern Analysis and Machine Intelligence*, vol. 37, no. 9, pp. 1751–1763, 2015.
- [20] T. Yokota, N. Lee, and A. Cichocki, "Robust multilinear tensor rank estimation using higher order singular value decomposition and information criteria," *IEEE Transactions on Signal Processing*, vol. 65, no. 5, pp. 1196–1206, 2017.
- [21] H. A. Kiers, "Towards a standardized notation and terminology in multiway analysis," *Journal of Chemometrics: A Journal of the Chemometrics Society*, vol. 14, no. 3, pp. 105–122, 2000.
- [22] C. J. Hillar and L.-H. Lim, "Most tensor problems are np-hard," *Journal of the ACM (JACM)*, vol. 60, no. 6, pp. 1–39, 2013.
- [23] L. R. Tucker, "Some mathematical notes on three-mode factor analysis," *Psychometrika*, vol. 31, no. 3, pp. 279–311, 1966.
- [24] J. Liu, P. Musialski, P. Wonka, and J. Ye, "Tensor completion for estimating missing values in visual data," *IEEE transactions on pattern analysis and machine intelligence*, vol. 35, no. 1, pp. 208–220, 2012.
- [25] B. Romera-Paredes and M. Pontil, "A new convex relaxation for tensor completion," *Advances in neural information processing systems*, vol. 26, 2013.
- [26] M. E. Kilmer and C. D. Martin, "Factorization strategies for third-order tensors," *Linear Algebra and its Applications*, vol. 435, no. 3, pp. 641–658, 2011.
- [27] Z. Zhang and S. Aeron, "Exact tensor completion using t-svd," *IEEE Transactions on Signal Processing*, vol. 65, no. 6, pp. 1511–1526, 2017.
- [28] Y.-B. Zheng, T.-Z. Huang, X.-L. Zhao, T.-X. Jiang, T.-Y. Ji, and T.-H. Ma, "Tensor n-tubal rank and its convex relaxation for low-rank tensor recovery," *Information Sciences*, vol. 532, pp. 170–189, 2020.
- [29] H. Kong, X. Xie, and Z. Lin, "t-schatten- p norm for low-rank tensor recovery," *IEEE Journal of Selected Topics in Signal Processing*, vol. 12, no. 6, pp. 1405–1419, 2018.
- [30] W.-H. Xu, X.-L. Zhao, T.-Y. Ji, J.-Q. Miao, T.-H. Ma, S. Wang, and T.-Z. Huang, "Laplace function based nonconvex surrogate for low-rank tensor completion," *Signal Processing: Image Communication*, vol. 73, pp. 62–69, 2019.
- [31] P. Gong, C. Zhang, Z. Lu, J. Huang, and J. Ye, "A general iterative shrinkage and thresholding algorithm for non-convex regularized optimization problems," in *international conference on machine learning*. PMLR, 2013, pp. 37–45.
- [32] J. You, Y. Jiao, X. Lu, and T. Zeng, "A nonconvex model with minimax concave penalty for image restoration," *Journal of Scientific Computing*, vol. 78, no. 2, pp. 1063–1086, 2019.
- [33] C.-H. Zhang, "Nearly unbiased variable selection under minimax concave penalty," *The Annals of statistics*, vol. 38, no. 2, pp. 894–942, 2010.
- [34] P. K. Pokala, R. V. Hemadri, and C. S. Seelamantula, "Iteratively reweighted minimax-concave penalty minimization for accurate low-rank plus sparse matrix decomposition," *IEEE Transactions on Pattern Analysis and Machine Intelligence*, 2021.
- [35] J. Fan and R. Li, "Variable selection via nonconcave penalized likelihood and its oracle properties," *Journal of the American statistical Association*, vol. 96, no. 456, pp. 1348–1360, 2001.
- [36] D. Qiu, M. Bai, M. K. Ng, and X. Zhang, "Nonlocal robust tensor recovery with nonconvex regularization," *Inverse Problems*, vol. 37, no. 3, p. 035001, 2021.
- [37] X. Zhang, "A nonconvex relaxation approach to low-rank tensor completion," *IEEE transactions on neural networks and learning systems*, vol. 30, no. 6, pp. 1659–1671, 2018.
- [38] X. Zhang, M. Bai, and M. K. Ng, "Nonconvex-tv based image restoration with impulse noise removal," *SIAM Journal on Imaging Sciences*, vol. 10, no. 3, pp. 1627–1667, 2017.
- [39] P. Ochs, A. Dosovitskiy, T. Brox, and T. Pock, "On iteratively reweighted algorithms for nonsmooth nonconvex optimization in computer vision," *SIAM Journal on Imaging Sciences*, vol. 8, no. 1, pp. 331–372, 2015.
- [40] J. Bolte, S. Sabach, and M. Teboulle, "Proximal alternating linearized minimization for nonconvex and nonsmooth problems," *Mathematical Programming*, vol. 146, no. 1, pp. 459–494, 2014.
- [41] C. Lu, J. Feng, Y. Chen, W. Liu, Z. Lin, and S. Yan, "Tensor robust principal component analysis with a new tensor nuclear norm," *IEEE Transactions on Pattern Analysis and Machine Intelligence*, vol. 42, no. 4, pp. 925–938, 2020.
- [42] Z. Zhang, G. Ely, S. Aeron, N. Hao, and M. Kilmer, "Novel methods for multilinear data completion and de-noising based on tensor-svd," *2014 IEEE Conference on Computer Vision and Pattern Recognition*, pp. 3842–3849, 2014.
- [43] R. T. Rockafellar and R. J.-B. Wets, *Variational analysis*. Springer Science & Business Media, 2009, vol. 317.
- [44] R. Tibshirani, "Regression shrinkage and selection via the lasso: a retrospective," *Journal of the Royal Statistical Society: Series B (Statistical Methodology)*, vol. 73, no. 3, pp. 273–282, 2011.
- [45] F. H. Clarke, *Optimization and nonsmooth analysis*. SIAM, 1990.
- [46] Z. Wang, A. Bovik, H. Sheikh, and E. Simoncelli, "Image quality assessment: from error visibility to structural similarity," *IEEE Transactions on Image Processing*, vol. 13, no. 4, pp. 600–612, 2004.
- [47] L. Zhang, L. Zhang, X. Mou, and D. Zhang, "Fsim: A feature similarity index for image quality assessment," *IEEE Transactions on Image Processing*, vol. 20, no. 8, pp. 2378–2386, 2011.
- [48] L. Wald, *Data fusion: definitions and architectures: fusion of images of different spatial resolutions*. Presses des MINES, 2002.
- [49] J. Liu, P. Musialski, P. Wonka, and J. Ye, "Tensor completion for estimating missing values in visual data," *IEEE Transactions on Pattern Analysis and Machine Intelligence*, vol. 35, no. 1, pp. 208–220, 2013.
- [50] X. Li, Y. Ye, and X. Xu, "Low-rank tensor completion with total variation for visual data inpainting," *Proceedings of the AAAI Conference on Artificial Intelligence*, vol. 31, no. 1, 2017.
- [51] T.-X. Jiang, T.-Z. Huang, X.-L. Zhao, and L.-J. Deng, "Multi-dimensional imaging data recovery via minimizing the partial sum of tubal nuclear norm," *Journal of Computational and Applied Mathematics*, vol. 372, p. 112680, 2020.
- [52] T.-X. Jiang, M. K. Ng, X.-L. Zhao, and T.-Z. Huang, "Framelet representation of tensor nuclear norm for third-order tensor completion," *IEEE Transactions on Image Processing*, vol. 29, pp. 7233–7244, 2020.
- [53] Y.-B. Zheng, T.-Z. Huang, X.-L. Zhao, T.-X. Jiang, T.-H. Ma, and T.-Y. Ji, "Mixed noise removal in hyperspectral image via low-fibered-rank regularization," *IEEE Transactions on Geoscience and Remote Sensing*, vol. 58, no. 1, pp. 734–749, 2019.
- [54] W. Cao, Y. Wang, C. Yang, X. Chang, Z. Han, and Z. Xu, "Folded-concave penalization approaches to tensor completion," *Neurocomputing*, vol. 152, pp. 261–273, 2015.
- [55] D. Goldfarb and Z. Qin, "Robust low-rank tensor recovery: Models and algorithms," *SIAM Journal on Matrix Analysis and Applications*, vol. 35, no. 1, pp. 225–253, 2014.